This is a post-peer-review, pre-copyedit version of an article published in American Mineralogist. The final authenticated version is available online at: http://dx.doi.org/10.2138/am-2016-5540

Error sources in single-clinopyroxene thermobarometry and a mantle geotherm for the Novinka kimberlite, Yakutia

Luca Ziberna[a,b] *, Paolo Nimis[b], Dmitry Kuzmin [c,d], Vladimir G. Malkovets[c,d]

[a] School of Earth Sciences, University of Bristol, Wills Memorial Building, Queen's Road, Bristol BS8 1RJ, United Kingdom

[b] Dipartimento di Geoscienze, Università di Padova, Via G. Gradenigo 6, 35131 Padova, Italy

[c] V. S. Sobolev Institute of Geology and Mineralogy, Siberian Branch of Russian Academy of Sciences, 3 Koptuyga prospect, Novosibirsk 630090, Russia

[d] Novosibirsk State University, 2 Pirogova Str., Novosibirsk 630090, Russia

ABSTRACT

A new suite of 173 clinopyroxene grains from heavy-mineral concentrates of the diamondiferous Novinka kimberlite (Upper Muna field, Yakutia) has been analyzed for major and minor elements with an electron microprobe to perform a thermobarometric study and model the thermal structure of the Proterozoic Upper Muna lithospheric mantle. Scrupulous evaluation of propagation of analytical uncertainties on pressure estimates revealed that (i) the single-clinopyroxene geobarometer can be very sensitive to analytical uncertainties for particular clinopyroxene compositions, and that (ii) most clinopyroxenes from Novinka have compositions that are sensitive to analytical uncertainties, notwithstanding their apparent compositional suitability for single-clinopyroxene thermobarometry based on previously proposed application limits. A test on a variety of mantle clinopyroxenes containing different proportions of the sensitive elements Cr, Na and Al allowed us to identify clinopyroxene compositions that produce unacceptably high propagated errors and to define appropriate analytical conditions (i.e., higher beam currents and longer counting times for specific elements) that allow precise *P–T* estimates to be obtained for sensitive compositions. Based on the results of our analytical test, and taking into account the intrinsic limitations of the single-

clinopyroxene thermobarometer, we have designed a new protocol for optimum thermobarometry, which uses partly revised compositional filters. The new protocol permits precise computation of the conductive paleogeotherm at Novinka with the single-clinopyroxene thermobarometer of Nimis and Taylor (2000). Thermal modeling of the resulting *P–T* estimates indicates a ~34-mW/m^2 surface heat flow, a thermal lithosphere thickness of ~225 km, and an over 100 km-thick 'diamond window' beneath Novinka in the middle Paleozoic (344–361 Ma). We estimate that appropriate analytical conditions may extend the applicability of single-clinopyroxene thermobarometry to over 90% of clinopyroxene-bearing garnet peridotites and pyroxenites and to ~70% of chromian-diopside inclusions in diamonds. In all cases, application to clinopyroxenes with $Cr/(Cr + Al)_{mol} < 0.1$ is not recommended. We confirm the tendency of the single-clinopyroxene barometer to progressively underestimate pressure at $P > 4.5$ GPa.

Keywords: Geobarometry, Chromian diopside, Lithospheric mantle, Palaeogeotherms

INTRODUCTION

Over the last few decades, thermobarometry of rocks and minerals derived from Earth's mantle has represented a fundamental tool for the evaluation of the thermal state and structure of sub-craton and off-craton lithospheric sections (e.g., Boyd 1973, 1984; O'Reilly and Griffin 1985; Boyd et al. 1997; Kopylova et al. 1998; Griffin et al. 1999, 2002, 2004; Lazarov et al. 2009; Janney et al. 2010), as well as for the assessment of their diamond potential (e.g., Read et al. 2004; Read and Janse 2009; Cookenboo and Grütter 2010). Deep-seated mantle samples mostly occur as discrete xenoliths or xenocrysts in alkaline magmatic rocks, as isolated grains in sediments derived from their weathering and disruption, and as monomineralic or polymineralic inclusions in kimberlite- and lamproite-borne diamonds. Only the relatively rare discrete xenoliths and polymineralic inclusions in diamonds may be suitable for conventional, two-phase thermobarometry. Single-mineral thermometer–barometer pairs, such as those available for peridotitic garnet and clinopyroxene (Ryan et al. 1996; Nimis and Taylor

2000; Grütter et al. 2006), permit thermobarometric surveys to extend across copious data for mantle-derived xenocrysts. Although with some limitations concerning their reliability and applicability (e.g., Cookenboo and Grütter 2010), the single-mineral methods have enabled the vertical and horizontal mapping of the lithospheric mantle to an extent far beyond that achievable with xenoliths alone (e.g., Griffin et al. 1999, 2002, 2004; Malkovets et al. 2007; Ashchepkov et al. 2008; Grütter and Tuer 2009; Lehtonen et al. 2009; Nimis et al. 2009; Zozulya et al. 2009).

The single-clinopyroxene thermobarometer of Nimis and Taylor (2000) is one of the most used and most reliable single-mineral methods for thermobarometry of disaggregated mantle xenoliths (Nimis 2002; Putirka 2008; Grütter 2009; Nimis and Grütter 2010), though its application requires judicious filtering of appropriate clinopyroxene compositions, as well as careful evaluation of the errors associated with calculated temperatures and pressures. Empirically determined compositional filters for single-clinopyroxene thermobarometry were proposed by Nimis and Taylor (2000) and endorsed by Grütter (2009), and low-quality microprobe data were highlighted as resposnsible for unreliable clinopyroxene thermobarometry outcomes (Grütter 2009; Mather et al. 2011). However, the source of the decreased reliability of single-clinopyroxene thermobarometry for particular compositions has never been investigated in detail. In this contribution, we assess the various sources of error that may affect single-clinopyroxene barometry and propose a new protocol for optimal single-clinopyroxene thermobarometry which specifically considers analytical errors and uses partly revised compositional filters. We then use our results to define a precise conductive geotherm for the diamondiferous Novinka kimberlite, Yakutia, based on high-quality electron microprobe analyses of 97 chromian diopside xenocrysts, selected out of an initial suite of 173 chromian diopside grains. We show that previously proposed compositional filters are sufficient for routine evaluation of mantle geotherms using data for large populations of mantle-derived clinopyroxenes, but that high-quality chemical analyses significantly improve the precision of the individual *P*-*T* estimates for fairly common chromian diopside compositions.

GEOLOGICAL OUTLINE AND PRELIMINARY SAMPLE SELECTION

The Upper Muna kimberlite field is located at the northern limb of the Markha Terrane, in the central part of the Siberian Craton, and is one of the thirteen fields that form the SW–NE Daldyn–Olenek kimberlite corridor (Fig. 1). This kimberlite field is composed of twenty kimberlite bodies intruded in the Upper Cambrian limestones of the sedimentary cover of the Siberian Platform and is related to the Late Devonian-Early Carboniferous episode of kimberlite magmatism on the Siberian platform (Davis et al. 1980; Agashev et al. 2004; Sun et al. 2014). Recent age determinations gave a narrow interval of kimberlite formation from 361 to 344 Ma (Griffin et al. 1999; Levchenkov et al. 2005; Lepekhina et al. 2008a,b; Malkovets VG, unpublished data). For the Novinka kimberlite, SHRIMP analyses of groundmass perovskites gave a U–Pb age of 355±11 Ma (Lepekhina et al. 2008b). One of the striking features of the Upper Muna kimberlite field is that most of the bodies are diamondiferous. All the kimberlite bodies are characterized by abundant fresh deep-seated xenocrysts and xenoliths, but eclogite and crustal xenoliths are very rare.

The samples for this study were collected from five sites in the quarry left after bulk sampling inside the contour of the pipe at the present surface and are believed to be a representative mixture of all exposed kimberlite types presently recognized at Novinka. A total of 173 fresh green clinopyroxene grains were picked from the 0.3 to 1.5-mm fraction of heavy-mineral concentrates separated using bromoform at the VS Sobolev Institute of Geology and Mineralogy, Siberian Branch Russian Academy of Sciences, Novosibirsk, Russia. Preliminary major element analyses were performed on these grains using a JEOL Superprobe JXA-8200 electron microprobe (hereafter, EMP) housed at the Max Planck Institute for Chemistry, Mainz, Germany. Operating conditions and compositions for all 173 grains are reported in the Supplementary Table S1.

OPTIMIZED PROTOCOL FOR PRECISE SINGLE-CLINOPYROXENE THERMOBAROMETRY

Source of errors and compositional filters

The single-clinopyroxene thermobarometer uses a combination of the enstatite-in-Cpx thermometer and Cr-in-Cpx barometer (Nimis and Taylor 2000). The enstatite-in-Cpx thermometer has proved a top-quality method when compared to other mantle geothermometers (Nimis and Grütter 2010) and has limited sensitivity to analytical uncertainties (Nimis 2002). The Cr-in-Cpx barometer suffers from two major drawbacks: i) evaluations against experiments have shown progressive underestimation of the equilibrium pressures above ca. 4.5 GPa (up to 0.6–1.0 GPa at 7.0 GPa; Nimis 2002); ii) deviations from results of orthopyroxene–garnet barometry on the same xenolith samples can be very large for clinopyroxenes characterized by low values of a_{Cr} = Cr – 0.81·(Na + K)·Cr/(Cr + Al) atoms per 6-oxygen formula unit (hereafter apfu), which is the main building block in the barometer formulation (Fig. 2). Low a_{Cr} values at high P/T ratios in the calibration database, a molar volume change for the reaction involving garnet and clinopyroxene (cf. equation 1 in Nimis and Taylor 2000) less than one-half that of common orthopyroxene-based barometers (cf. Brey et al. 1990), and the intrinsic limitations of being an empirical single-mineral method account for the lower precision of the Cr-in-Cpx barometer (cf. Figs. 1c,d in Grütter 2009). More generally, these drawbacks may explain why P–T estimates using the single-clinopyroxene methods are often more scattered compared to those using conventional thermobarometers (cf. Stachel and Harris 2008; Eaton et al. 2009; Shirey et al. 2013).

Apart from the above issues, safe application of the single-clinopyroxene method requires a careful selection of the samples, in order to exclude compositions outside the range used for the calibration or too sensitive to analytical uncertainties. Grütter (2009) compiled and partly modified compositional and related filters designed by various authors that serve as a useful ‘cookbook’ to eliminate unwarranted data from consideration for P-T calculations. The filters include: (i) total cations per 6 oxygens in the range 3.96–4.04, slightly more permissive than the 3.98–4.02 range advised by Nimis and Taylor (2000); (ii) Cr_2O_3 vs Al_2O_3 relationships within the garnet-peridotite field of Ramsay and

127 Tompkins (1994); (iii) Al_2O_3 vs MgO relationships within the high-Al field of Nimis (1998); (iv) *Cr#*
128 in the range 0.06–0.50; (v) $a_{Cr} \geq 0.003$ apfu. Filter (i) serves to exclude obviously poor-quality
129 analyses, which may result from poor EMP standardization, bad sample preparation, contamination
130 from inclusions, etc. In this work we revert to the more restrictive 3.98–4.02 cation range to promote
131 high-quality *P–T* estimates for individual clinopyroxene grains. Filters (ii) and (iii) serve to exclude
132 clinopyroxenes that may not have been in equilibrium with garnet. Filters (iv) and (v) exclude
133 compositions falling well outside the range of the experiments used for the calibration of the Cr-in-Cpx
134 barometer, which included clinopyroxenes with *Cr#* = 0.09–0.44, and a_{Cr} = 0.003–0.087 apfu (Nimis
135 and Taylor 2000). As originally suggested by Nimis and Taylor (2000), the removal of clinopyroxenes
136 with $a_{Cr} < 0.003$ apfu should also help to exclude compositions that are too sensitive to propagation of
137 analytical errors. We will show that filters (iv) and (v) require revision.
138 Figure 2 shows that the threshold $a_{Cr} \geq 0.003$ apfu suggested by Nimis and Taylor (2000) and
139 adopted by Grütter (2009) may be too optimistic: at a_{Cr} = 0.010 apfu, deviations from the
140 orthopyroxene–garnet pressures calculated for the same well-equilibrated mantle xenoliths may be as
141 high as ±1.0 GPa, reaching ±3.0 GPa for $a_{Cr} < 0.003$ apfu. This shortcoming is particularly relevant for
142 the study of Novinka chromian diopsides. Based on preliminary microprobe analyses of 173 grains
143 (Supplementary Table S1), 118 grains satisfy the compositional criteria for derivation from garnet
144 peridotite [i.e., filters (ii) and (iii)], with 39 of 118 (33%) having $a_{Cr} \leq 0.003$ apfu, and 107 of 118
145 (91%) having $a_{Cr} \leq 0.010$ apfu. Observing the latter threshold would therefore render most of our
146 Novinka samples unsafe for thermobarometry. In principle, the decreased precision of the Cr-in-Cpx
147 barometer at low a_{Cr} may be due to an oversimplified treatment of Cr equilibria between clinopyroxene
148 and garnet or it may reflect an excessive sensitivity of the method to analytical errors or to departures
149 from chemical equilibrium. Mather et al. (2011) made a semi-quantitative evaluation of the influence of
150 analytical errors, but they did not account for their dependence on absolute element concentrations and

151 analytical conditions (cf. Potts 1983 and Appendix of this work). In the present work, we have made an
152 analytical test to quantitatively assess the propagation of analytical errors on pressure estimates (see
153 Appendix for details): multiple EMP analyses on compositionally diverse clinopyroxenes using
154 different analytical conditions demonstrated that (i) the decreased precision of the Cr-in-Cpx barometer
155 for clinopyroxenes with low a_{Cr} values is largely related to propagation of analytical errors, (ii) the
156 analytical errors, as expected, increase smoothly with decreasing beam current and counting times, and
157 (iii) the propagated *P* uncertainties are negatively correlated with the clinopyroxene a_{Cr} parameter and
158 positively correlated with the clinopyroxene Cr/(Cr + Al) molar ratio (*Cr#*) (Fig. 3). Therefore, the
159 a_{Cr}/*Cr#* parameter, rather than the previously used a_{Cr} parameter, is a more reliable indicator of the
160 sensitivity of single-clinopyroxene barometry to analytical uncertainties. Minimum conditions for
161 electron microprobe analysis were thus defined for different values of the a_{Cr}/*Cr#* parameter (Table
162 A2), which maintain propagation of analytical uncertainties within acceptable limits (defined here as ±
163 0.25 GPa).

164 A further assessment of the importance of analytical errors on Cr-in-Cpx *P* estimates can be made
165 using mantle xenoliths as test cases. Based on the results of our analytical tests (see Appendix), we
166 have refined the database of well-equilibrated xenoliths of Nimis and Grütter (2010) by excluding those
167 clinopyroxene analyses for which the estimated *P* uncertainties were unsatisfactorily high. For each
168 record, the analytical errors on Al, Cr, and Na concentrations in the clinopyroxene were calculated
169 taking into account the analytical conditions used for the analysis as reported in the source papers, and
170 the corresponding *P* uncertainties were calculated through error propagation. If the reported analytical
171 conditions did not match exactly any of those utilized here, the errors were estimated by interpolation
172 of values obtained by assuming lower and higher beam currents or counting times. For records for
173 which analytical details had not been reported, we cautiously assumed the beam current and counting
174 times to be the lowest (i.e., 15 nA, 10 s peak, 10 s background). The records for which the model *P*
175 uncertainties were greater than ± 0.25 GPa were discarded. Clearly, the model *P* uncertainties may not

176 be strictly accurate, since different analytical equipments were used for the analyses. However, the
177 above screening certainly excluded most of the records for which single-clinopyroxene *P–T* estimates
178 are probably unreliable. Figure 4 shows that the discrepancies between Cr-in-Cpx and orthopyroxene–
179 garnet pressures are greatly reduced for the refined database, especially at pressures above 3 GPa, thus
180 supporting the major role of propagation of analytical errors on *P* uncertainties. At lower pressures,
181 significant deviations are still observed only for a few samples with $Cr\# < 0.1$ (Fig. 4b), which suggests
182 poor reliability of the Cr-in-Cpx barometer for these low-*Cr*# compositions. This may be related to the
183 fact that the Cr-in-Cpx barometer was calibrated on 120 experimental clinopyroxenes with *Cr*# in the
184 range 0.09–0.44, with only 6 of them having $Cr\# < 0.1$ (Nimis and Taylor 2000). The original
185 minimum threshold of 0.06 for *Cr*# suggested by Grütter (2009) thus appears to be too permissive.
186 Examination of Figure 4b also reveals that clinopyroxenes with *Cr*# as high as 0.65 do not show any
187 systematic deviation from orthopyroxene–garnet *P*. This suggests that the upper limit for *Cr*# of 0.50
188 proposed by Grütter (2009) is excessively restrictive, despite the fact that the Cr-in-Cpx barometer was
189 calibrated on clinopyroxenes with $Cr\# \leq 0.44$.

190 An additional problem when investigating loose mineral grains is to assess whether the
191 clinopyroxene was in equilibrium with orthopyroxene, a condition necessary for single-clinopyroxene
192 thermometry. Recognition of orthopyroxene-saturated samples is not straightforward and was not
193 explicitly addressed by Grütter (2009). Based on the above considerations, we propose a partly revised
194 protocol for sample selection, which takes into account both the intrinsic limitations of the single-
195 clinopyroxene thermobarometers and the uncertainties related to propagation of analytical errors.

196 (1) *General quality test of EMP analysis*: total cations per 6 oxygens in the range 3.98–4.02. Less
197 restrictive limits, such as those suggested by Grütter (2009), might be adopted in some cases, but a
198 possible increase of scatter around geotherms should be considered.

199 (2) *General equilibrium test*: grains exhibiting significant zoning, suggesting disequilibrium,
200 should generally be discarded.

(3) *Verification of equilibrium with garnet*: Cr_2O_3 vs Al_2O_3 relationships within the garnet-peridotite field of Ramsay and Tompkins (1994), i.e., $Cr_2O_3 > 0.5$ wt% *and* $Al_2O_3 \leq 4.0$ wt% (if $Cr_2O_3 < 2.25$ wt%) or ≤ 5.0 wt% (if $Cr_2O_3 > 2.25$ wt%). This restriction may produce false negatives. The reliability of single-clinopyroxene methods for anomalously Cr_2O_3-rich compositions ($Cr_2O_3 > 5.0$ wt%) is unknown and therefore these compositions should be used with caution.

(4) *Further refinement of (3)*: Al_2O_3 vs MgO relationships within the high-Al field of Nimis (1998), i.e., $Al_2O_3 \geq 0.7$ wt% *and* $Al_2O_3 \geq 12.175 - 0.6375$*MgO wt% (this parametrization is taken directly from Fig. 3 in Nimis 1998; the slightly different formula suggested by Grütter 2009 provides almost identical results). False negatives may be produced also in this case, especially among diamond-facies samples (cf. Fig. 3 in Nimis 1998).

(5) *Rejection of compositions with 'unsafe' Cr# values*: *Cr#* in the range 0.10–0.65 (replacing the range 0.06–0.50 of Grütter 2009); *Cr#* values in the range 0.50–0.65 should still be used with caution because of limited testing in this compositional range.

(6) *Recognition of compositions sensitive to analytical uncertainties*: $a_{Cr}/Cr\# > x$, where x is a function of EMP analytical conditions. Table A2 provides a general guideline for determining x, although its value may be varied for different analytical equipments based on personal experience. This filter replaces the filter $a_{Cr} \geq 0.003$ apfu of Nimis and Taylor (2000) and Grütter (2009). If $a_{Cr}/Cr\# \leq 0.011$ apfu, the clinopyroxenes should generally be discarded; if $0.011 < a_{Cr}/Cr\# \leq 0.024$ apfu, high-quality analyses are recommended; if $a_{Cr}/Cr\# > 0.024$, propagation of analytical errors is predictably small and therefore routine analyses can safely be used. The range for $a_{Cr}/Cr\#$ in the experiments used to calibrate the Cr-in-Cpx barometer of Nimis and Taylor (2000) was 0.016–0.393, therefore excluding compositions with $a_{Cr}/Cr\# \leq 0.011$ apfu will also avoid large extrapolations outside the calibration range.

(7) *Verification of equilibrium with orthopyroxene*. This cannot be obtained through simple compositional filters. In general, $Ca/(Ca + Mg)_{mol}$ ratios > 0.5 should be considered as suspicious, as a very small proportion of orthopyroxene-saturated chromian diopsides (ca. 1%) lie above this value. A very low estimated *T* (e.g., <600 °C) would also be a strong indication that the diopside was not in equilibrium with orthopyroxene, which implies underestimation of *T* using the enstatite-in-Cpx thermometer and, consequently, underestimation of the Cr-in-Cpx *P*. Following Nimis and Grütter (2010), a cut-off at *T* > 700°C provides a safer selection of clinopyroxenes for which enstatite-in-Cpx temperatures should be sufficiently reliable.

(8) *Identification of potential outliers.* As recommended by Grütter (2009), final examination of *P*–*T* plots for a given locality may help to distinguish outliers departing off the general trend, which may conveniently be excluded for the determination of mantle geotherms.

Application to Novinka clinopyroxenes

For the purposes of this study, we used the preliminary analyses of Novinka clinopyroxenes (Jeol Superprobe, Mainz; Supplementary Table S1) only for a first compositional screening aimed to eliminate obviously unsuitable analyses. We excluded 55 clinopyroxenes plotting outside the 'garnet peridotite' field of Ramsay and Tompkins (1994), which may not be equilibrated with garnet, and 5 clinopyroxenes showing very low enstatite contents [$Ca/(Ca + Mg)_{mol}$ > 0.5], which are unlikely to be equilibrated with orthopyroxene. In addition, 16 grains that contained abundant melt inclusions, which likely indicate severe interaction with the host kimberlite magma, were also discarded.

The remaining 97 grains were re-analysed using a CAMECA SX-50 electron microprobe (EMP; IGG–CNR, Padua, Italy) (see Appendix for details). Compositional data were first collected using a *routine* analytical procedure, which employed an accelerating voltage of 20 kV, a beam current of 15 nA, and counting times of 10 s for peak and 10 s for background (i.e., 5 s on each side of the peak), for all elements. Further filtering based on the newly revised protocol was then applied to the results of the

249 routine analyses. We discarded 5 grains showing significant zoning, 9 grains plotting outside the high-
250 Al field of Nimis (1998) and 9 grains showing $a_{Cr}/Cr\# < 0.011$. We then re-analyzed 56 clinopyroxenes
251 with $0.011 < a_{Cr}/Cr\# \leq 0.024$ using higher beam current (40 nA) and counting times (40 sec for both
252 peak and background) for Al, Cr and Na, and routine EMP conditions for the other elements. Pressures
253 and temperatures were calculated with the thermobarometers of Nimis and Taylor (2000) using the
254 averages of five point analyses. The major element compositions of the peridotitic clinopyroxenes
255 determined using both the routine and the optimized analytical conditions and the relative *P–T*
256 estimates are reported in the Supplementary Table S2.
257
258 **RESULTS**
259 Based on the preliminary analyses of the 173 clinopyroxenes (Supplementary Table S1), the majority
260 of the grains (68%) fall into the low-Al, 'garnet peridotite' field of Ramsay and Tompkins (1994).
261 About one fourth of these, however, show relationships between Al_2O_3 and MgO contents that are
262 compatible also with an origin from garnet-free, metasomatised lherzolites (cf. Nimis 1998). Another
263 4% fraction of the 'garnet peridotite' grains shows high CaO contents (>22 wt.%), high $Ca/(Ca + Mg)_{mol}$ ratios (>0.5) and excessively low estimated *T* (<500 °C) and can be classified as 'wehrlitic'. A
265 relatively large number of the studied grains (29%) have Cr_2O_3 contents lower than 0.5 wt.%, which
266 would classify them as either 'eclogitic' or 'megacrystic' (Ramsay and Tompkins 1994). The Na_2O
267 content in these low-Cr grains is generally low to very low (mostly <2.5 wt.%), which is more
268 consistent with a megacrystic/pyroxenitic origin. A very small number of grains (2%) have relatively
269 high Al_2O_3 contents (4.6–5.4 wt.%) and fall in the spinel peridotite field of Ramsay and Tompkins
270 (1994).
271 Grey symbols in Figure 5a show the results of the thermobarometric study of the 97 selected
272 clinopyroxenes using the routine analyses obtained with the CAMECA SX50 (Padua). As expected
273 from the low a_{Cr} values of most clinopyroxenes, the *P–T* estimates obtained using routine analyses

show considerable scatter, especially at $P > 5.0$ GPa (Fig. 5a). Depending on the preferred model geotherm shape, minor to very large thermal perturbations (up to several hundred degrees) may be inferred near the base of the lithosphere. Adopting the revised filtering protocol proposed in this work and using 56 high-quality analyses for clinopyroxenes with $0.011 < a_{Cr}/Cr\# \leq 0.024$, the *P*-*T* scatter is considerably reduced (black symbols in Fig. 5a). Ten samples with $Cr\# > 0.50$ and as high as 0.63 do not show any deviation from the overall trend, which supports the reliability of single clinopyroxene thermobarometry for these compositions (cf. also Fig. 4). The refined thermobarometric estimates (N = 74) span the *P*–*T* range 2.3–6.5 GPa and 660–1390 °C, with the majority of the clinopyroxenes falling in the diamond stability field (Fig. 5a). Trimming the data at $T > 700$ °C does not produce any reduction in the overall scatter. A gap is observed in the pressure range 3.3–3.9 GPa, which could be related to a sampling bias of the kimberlite or to absence of clinopyroxene-saturated assemblages in the mantle in this pressure interval.

For the sake of comparison, Figure 5b shows the results of the thermobarometric study of the same 97 clinopyroxenes, but adopting Grütter's (2009) original filters for $Cr\#$ ($0.06 < Cr\# < 0.5$) and a_{Cr} (≥ 0.003 apfu) and using routine analyses for all samples. The results show a marginal increase of scatter and an overall shift of the high-*P* samples (> 4.0 GPa) to slightly higher *P*, the average difference being ca. 0.2 GPa. However, differences in *P*–*T* estimates for individual grains (routine vs. high-quality analyses) are as high as +0.5 GPa and +50 °C and the total number of 'accepted' clinopyroxenes is reduced to 67.

THERMAL STATE AND THICKNESS OF THE UPPER MUNA LITHOSPHERIC MANTLE

Much of what is known about the thermal state of the mantle beneath the Siberian craton comes from studies of xenoliths from the Daldyn field (Fig. 1), and in particular from the Udachnaya kimberlite. Conventional thermobarometry of mantle xenoliths from this kimberlite indicates low geothermal gradients, corresponding to a surface heat flow of 35–40 mW/m^2 based on the conductive model of

299 Pollack and Chapman (1977) (hereafter PC77), and deep lithospheric mantle roots (~ 220 km) (Griffin
300 et al. 1996; Boyd et al. 1997; Pokhilenko et al. 1999; Ionov et al. 2010; Goncharov et al. 2012;
301 Agashev et al. 2013; Doucet et al. 2013). Variations in available estimates of the (conductive) mantle
302 geotherm depend in part on the different combinations of thermobarometers used by the different
303 authors and in part on a significant scatter in the reported *P–T* estimates.

304 Additional slices of information on the Daldyn field and on the nearby Alakit and Upper Muna
305 fields (Fig. 1) were provided by Griffin et al. (1999), who applied the Ni-in-garnet thermometer and
306 Cr-in-garnet barometer (Ryan et al. 1996) to large suites of garnet xenocrysts. Their results suggest a
307 cool geotherm (35 mW/m^2) and a chemical lithosphere thickness of ~240 km for the Alakit mantle
308 section, similar to that in the Daldyn mantle section, but a slightly higher geotherm (38 mW/m^2) and a
309 thinner lithosphere (~210 km) for the more northeasterly Upper Muna mantle section. The main
310 limitation of the garnet-based method is that reliable pressure estimates can only be retrieved for Cr-
311 saturated garnets (i.e., garnets in equilibrium with chromite). If this condition is not satisfied, only
312 minimum pressures can be estimated. Therefore, a geotherm is typically obtained by interpolating
313 maximum *P* estimates determined for each *T* recorded by a large number of grains. Scatter of
314 individual *P–T* points and intrinsic uncertainties in the empirical thermobarometer calibrations (Ryan et
315 al. 1996; Canil 1999), however, may limit the accuracy of the interpolation. Moreover, since Cr-
316 saturated garnets are relatively rare in kimberlites and their vertical distribution is not uniform (Griffin
317 et al. 2002; Malkovets et al. 2007), localized thermal perturbations are not easily recognized. More
318 recent *P–T* estimates for the Upper Muna field were provided by Ashchepkov et al. (2010), using
319 combinations of different thermobarometers. The results were ambiguous, because of the very large
320 scatter of *P–T* estimates and evident inconsistencies among the different thermobarometers used (see
321 Figs. 18 to 20 in Ashchepkov et al. 2010).

322 Our *P–T* data for clinopyroxenes provide independent constraints on the thermal state of the Upper
323 Muna lithospheric mantle at the time of eruption of the Novinka kimberlite. Figure 5 shows that the

low-T (< 1100 °C) clinopyroxenes align along the 40-mW/m^2 model conductive geotherm of PC77, which is slightly warmer than the 'garnet geotherm' defined by Griffin et al. (1999) for the Upper Muna field (38 mW/m^2). This is consistent with the observations of Grütter et al. (2006), who demonstrated that the Ni-in-garnet method of Ryan et al. (1996) adopted by Griffin et al. (1999) tends to underestimate mantle geotherms by ~2 mW/m^2. An apparent inflection of the geotherm is observed at T > 1100 °C and P > 5.5 GPa, with P–T data plotting on or slightly above the 44-mW/m^2 model conductive geotherm (Fig. 5a). This apparent inflection may partly be an artifact caused by the known P underestimation at high pressures of the Cr-in-Cpx geobarometer (cf. Nimis 2002; see also next Section). More importantly, the still widely used PC77 reference model predicts a stronger curvature of geotherms compared with recent thermal models (cf. Hasterok and Chapman 2011; Mather et al. 2011), and could suggest deviation from a conductive thermal gradient even in unperturbed mantle sections.

To derive a robust geotherm for the Upper Muna field, we have fitted the clinopyroxene P–T data using the FITPLOT program (McKenzie and Bickle 1988; McKenzie et al. 2005), as upgraded by and described in Mather et al. (2011). Different from the PC77 reference geotherms, this program allows computing the change in temperature with depth within the thermal boundary layer, allows varying the crustal thickness and heat production in the crust and mantle, and includes updated models for the temperature dependence of thermal conductivity. Moreover, the surface heat flow is an output of the fitting procedure and not a fixed input value that is used to generate a geotherm. We assumed a crustal thickness of 56 km based on Manakov's (2002) seismic model for the Siberian craton. The mean heat production in the crust was assumed to be 0.36 μW/m^3, in agreement with data reported in Rosen et al. (2009) for the Anabar shield. The heat production rate in the upper mantle was imposed at 0.0 μW/m^3 and the potential T for the asthenospheric isentrope was set at 1315 °C, following Mather et al. (2011). The thermal conductivity was assumed to be 2.5 W/m·K throughout the crust. In the mantle, we used the thermal conductivity for olivine at (P, T) of Osako et al. (2004).

348 Comparison of the clinopyroxene *P–T* data with the calculated geotherm (Fig. 6a) shows an
349 excellent agreement in the intermediate *P–T* region, with a residual 'inflection' at high *P–T*. The
350 magnitude of this inflection is compatible with the above-mentioned underestimation of the Cr-in-Cpx
351 barometer at high *P* (Nimis 2002; see also next Section). Therefore, we interpret the smooth high-*P–T*
352 inflection as an artifact. To minimize the potential bias due to *P* underestimation at high *P* and derive a
353 more refined geotherm, we have re-fitted the *P–T* data by excluding data plotting above 5.5 GPa.
354 Trimming the data did not produce significant changes in the model geotherm, excepting for an
355 obvious significant reduction of the xenolith misfit and a very slight increase in the calculated
356 lithospheric thickness, as defined by the intersection of the conductive geotherm with the mantle
357 isentrope (Fig. 6b). The agreement between the trimmed *P–T* data and the model is excellent. The
358 resulting surface heat flow is 34 mW/m^2 and the base of the thermal lithosphere is at 225 km,
359 corresponding to a *T* of 1436 °C. The base of the Mechanical Boundary Layer (McKenzie and Bickle
360 1988) is at 204 km depth, corresponding to a *T* of 1355 °C. Hasterok and Chapman's (2011) geotherm
361 model, which uses a more generalized heat production model for the continental lithosphere, would
362 also provide a good fit to the *P–T* data and would only suggest a slightly higher surface heat flux of 37
363 mW/m^2. The computed heat flow is slightly lower than that estimated by simple visual comparison
364 with the PC77 model geotherms (Fig. 6), but it is still significantly higher than the present-day value of
365 ~27 mW/m^2 (Duchkov and Sokolova 1997). Adopting different cut-off thresholds at high and low *P–T*
366 did not result in significant modification of the calculated geotherm. The combination of lithosphere
367 thickness and geothermal gradient indicates a large 'diamond window' beneath Novinka, extending
368 from ca. 110 to over 200 km depth in the middle Paleozoic (344–361 Ma).
369 Comparison with thermobarometric data for the nearby, broadly coeval (342–360 Ma; Davis et al.
370 1980) Daldyn kimberlite field (Figs. 6c–e) is hampered by the recognized temperature gap between ca.
371 900 and 1200 °C in *P–T* estimates for xenoliths from Udachnaya (Doucet et al. 2013), which reduces
372 the robustness of geotherm fitting, and by non-optimized analytical procedures in the literature data.

373 Additional ambiguity derives from minor inconsistencies between estimates obtained using different
374 thermobarometer pairs (cf. Doucet et al. 2013). If the same single-clinopyroxene thermobarometers are
375 used for both data sets, the *P–T* data for Udachnaya appear to be broadly consistent with the Upper
376 Muna calculated geotherm, although somewhat more scattered at high *T* (Fig. 6e).
377
378 **GENERAL IMPLICATIONS ON XENOLITH THERMOBAROMETRY AND GEOTHERM EVALUATION**
379 We have shown that careful compositional screening and high-quality analysis of peridotitic
380 clinopyroxenes from the Novinka kimberlite (Upper Muna field, Yakutia) have allowed to reduce
381 thermobarometric uncertainties and to make a good assessment of the thermal state of the lithospheric
382 mantle at the time of kimberlite eruption. It is worth noting, however, that EMP analytical conditions
383 employed in studies of garnet peridotites or diamond inclusions are often not optimized for reliable
384 thermobarometry. Moreover, in many cases, the analytical conditions are not reported or only partial
385 documentation is given. Of twenty-two published papers in which the Cr-in-Cpx barometer is applied
386 and documentation of EMP analytical conditions is provided, twenty used relatively low beam currents
387 (≤ 20 nA) and/or low counting times (≤ 20 s for peak) (e.g., Wang and Gasparik 2001; Menzies et al.
388 2004; Donnelly et al. 2007; Faryad et al. 2009; Nimis et al. 2009; Doucet et al. 2013; Chen et al. 2014).
389 This casts doubts on the reliability of many existing single-clinopyroxene thermobarometric data and
390 demands proper evaluation of propagation of analytical errors on *P* estimates.
391 Although analytical uncertainties will obviously depend not only on the adopted analytical
392 conditions but also on the performance of the equipment and quality of the standardization routines,
393 simplified thresholds based on compositional parameters reported in Table A2 can be used in common
394 practice to define the most appropriate analytical conditions for thermobarometric applications or to
395 help select the most reliable analyses from published datasets. If low beam current and short counting
396 times are used (e.g., 15 nA, 10 s peak, 10 s background), the safety threshold of $a_{Cr}/Cr\# > 0.024$ apfu
397 would cut off 19% of the 764 records in the mantle xenolith database of Nimis and Grütter (2010) and

46% of reported clinopyroxene inclusions in peridotitic and websteritic diamonds (cf. Stachel and Harris 2008). Using higher beam current and longer counting times (e.g., 40 nA, 40 s peak, 40 s background) the threshold may decrease to 0.011 apfu, thus cutting off only 4% of the xenoliths and 15% of the inclusions. The *Cr#* threshold of 0.1 proposed here cuts off further 5% of the xenoliths (mostly pyroxenites) and 17% of the inclusions (almost all from websteritic diamonds). Note that the $a_{Cr}/Cr\#$ ratio decreases with increasing P/T ratio (Fig. 7). Therefore, clinopyroxenes with compositions that are the most sensitive to propagation of analytical errors on estimated *P* (i.e., those with the lowest $a_{Cr}/Cr\#$) are those equilbrated under conditions corresponding to the highest P/T ratios. This indicates that clinopyroxene geotherms will tend to be less precise for cold cratonic mantle sections if EMP analyses are not of sufficient quality.

The effect of poor-quality analyses will tend to average out when a large population of chromian diopsides from a certain locality is used. Therefore, definition of mantle thermal state and diamond potential using the sample selection and analytical strategies proposed here may show only marginal improvement with respect to previously proposed protocols (cf. Grütter 2009). Nonetheless, the proportion of 'accepted' samples can be increased, the precision of individual *P–T* estimates can be improved, and 'unsafe' compositions are more effectively recognized (Fig. 5). This represents an advantage when the available population of clinopyroxene data is restricted for some reason (e.g. inclusions in diamonds), or when a detailed comparison between individual *P–T* estimates is required.

It should be emphasized that high-quality analyses *and* appropriate compositional screening will considerably reduce scatter of *P–T* estimates, but they will not eliminate systematic deviations of Cr-in-Cpx pressures due to inconsistencies in its calibration. In fact, the progressive negative deviation of Cr-in-Cpx *P* estimates relative to orthopyroxene–garnet *P* estimates at $P > 4.5$ GPa (Fig. 4) confirms the tendency of the Cr-in-Cpx barometer to underestimate at high *P* (by ca. 1 GPa at 7 GPa), which was previously observed against a limited set of experimental data (cf. Nimis 2002). Moreover, a slight positive deviation of the Cr-in-Cpx pressures (<0.5 GPa on average) is observed at *P* around 3 GPa

(Fig. 4), which partly confirms observations by Grütter and Moore (2003) and Grütter (2009). It is unclear if this small discrepancy at moderate *P* is due to inaccuracy of the Cr-in-Cpx barometer, of the orthopyroxene–garnet barometer, or of both. Owing to these systematic deviations, mantle palaeogeotherms calculated on the basis of single-Cpx thermobarometry will tend to show slightly different shapes than those based on orthopyroxene–garnet barometry. The most important discrepancies will affect the deepest portion of the lithosphere, where clinopyroxene geotherms will tend to show slightly overestimated *T*/*P* gradients. As discussed by Nimis (2002), this drawback will not hamper recognition of samples coming from the diamond window.

Acknowledgments

The present work is part of LZ's PhD research program at the University of Padova (Italy). The authors are indebted to G. Pearson, L. Franz and to late J. Boyd for supplying materials for the present study, and to R. Carampin (IGG-CNR, Padova) for his invaluable help during analytical sessions. H. Grütter and T. Stachel are thanked for sharing their compilations of xenolith and diamond inclusion data. S. Klemme is thanked for precious suggestions. Formal reviews by H. Grütter and an anonymous referee pointed out some important flaws in our original manuscript and helped us significantly improve this paper. PN acknowledges support by ERC Starting Grant 307322 (project INDIMEDEA). LZ acknowledges support by Fondazione Cassa di Risparmio di Padova e Rovigo – "Progetto Dottorati di Ricerca 2009". We thank A.V. Sobolev for the given opportunity to perform analytical procedures at the EPMA laboratory of the Max Planck Institute for Chemistry. VM and DK were supported by Russian Foundation for Basic Research (grant No. 16-05-01052). VM was supported by state assignment project No. 0330-2016-0006 and by Russian Science Foundation (grant No. 16-17-10067).

REFERENCES

Agashev, A.M., Pokhilenko, N.P., Tolstov, A.V., Polyanichko, V.V., Malkovets, V.G., Sobolev, N.V., 2004. New age data on kimberlites from the Yakutian diamondiferous province. Doklady Akademii Nauk SSSR, Earth Science Section 399, 1142–1145.

Agashev, A.M., Ionov, D.A., Pokhilenko, N.P., Golovin, A.V., Cherepanova, Y., and Sharygin, I.S. (2013) Metasomatism in lithospheric mantle roots: Constraints from whole-rock and mineral chemical composition of deformed peridotite xenoliths from kimberlite pipe Udachnaya. Lithos, 160-161, 201-215.

Ashchepkov, I.V., Pokhilenko, N.P., Vladykin, N.V., Logvinova, A.M., Afanasiev, V.P., Pokhilenko, L.N., Kuligin, S.S., Malygina, E.V., Alymova, N.A., Kostrovitsky, S.I., Rotman, A.Y., Mityukhin, S.I., Karpenko, M.A., Stegnitsky, Y.B., and Khemelnikova, O.S. (2010) Structure and evolution of the lithospheric mantle beneath Siberian craton, thermobarometric study. Tectonophysics, 485, 17-41.

Ashchepkov, I.V., Pokhilenko, N.P., Vladykin, N.V., Rotman, A.Y., and Afanasiev, V.P. (2008) Reconstruction of mantle sections beneath Yakutian kimberlite pipes using monomineral thermobarometry. Geological Society Special Publications, 293, 335-352.

Boyd, F.R. (1973) A pyroxene geotherm. Geochimica et Cosmochimica Acta, 37, 2533-2546.

Boyd, F.R. (1984) A Siberian geotherm based on lherzolite xenoliths from the Udachnaya kimberlite, U.S.S.R. Geology, 12, 528-530.

Boyd, F.R., Pokhilenko, N.P., Pearson, D.G., Mertzman, S.A., Sobolev, N.V., and Finger, L.W. (1997) Composition of the Siberian cratonic mantle: evidence from Udachnaya peridotite xenoliths. Contributions to Mineralogy and Petrology, 128, 228-246.

Canil, D. (1999) The Ni-in-garnet geothermometer: calibration at natural abundances. Contributions to Mineralogy and Petrology, 136, 240-246.

Carswell, D.A. (1991) The garnet–orthopyroxene Al barometer: problematic application to natural garnet lherzolite assemblages. Mineralogical Magazine, 55, 19-31.

Chen, M.M, Tian, W., Suzuki, K., Tejada, M.L.G., Liu, F.L., Senda, R., Wei, C.J., Chen, B., and Chu, Z.Y. (2014) Peridotite and pyroxenite xenoliths from Tarim, NW China: Evidences for melt depletion and mantle refertilization in the mantle source region of the Tarim flood basalt. Lithos, 204, 97-111.

Cookenboo, H.O., and Grütter, H.S. (2010) Mantle-derived indicator mineral compositions as applied to diamond exploration. Geochemistry: Exploration, Environment, Analysis, 10, 81-95.

Davis, G.L., Sobolev, N.V., and Khar'kiv, A.D. (1980) New data on the age of Yakutian kimberlites obtained by the uranium–lead method on zircons (in Russian). Doklady AN SSSR, 254, 175-180.

Day, H.W. (2012) A revised diamond-graphite transition curve. American Mineralogist, 97, 52-62.

Donnelly, C.L., Stachel, T., Creighton, S., Muehlenbachs, K., and Whiteford, S. (2007) Diamonds and their mineral inclusions from the A154 South pipe, Diavik Diamond Mine, Northwest territories, Canada. Lithos, 98, 160-176.

Doucet, L.S., Ionov, D.A., and Golovin, A.V. (2013) The origin of coarse garnet peridotites in cratonic lithosphere: new data on xenoliths from the Udachnaya kimberlite, central Siberia. Contributions to Mineralogy and Petrology, 165, 1225-1242.

Duchkov, A.D., and Sokolova, L.S. (1997) Thermal pattern of the lithosphere of the Siberian Platform (in Russian). Geologiya i Geofizika, 38, 494-503.

Eaton, D.W., Darbyshire, F., Evans, R.L., Grütter, H., Jones, A.G., and Yuan, X. (2009) The elusive lithosphere–asthenosphere boundary (LAB) beneath cratons. Lithos, 109, 1-22.

Faryad, S.W., Dolejš, D., and Machek, M. (2009) Garnet exsolution in pyroxene from clinopyroxenites in the Moldanubian zone: constraining the early pre-convergence history of ultramafic rocks in the Variscan froge. Journal of Metamorphic Geology, 27, 655-671.

494 Goncharov, A.G., Ionov, D.A., and Doucet, L.S. (2012) Thermal state, oxygen fugacity and C-O-H
495 fluid speciation in cratonic lithospheric mantle: new data on peridotite xenoliths from the
496 Udachnaya kimberlite, Siberia. Earth and Planetary Science Letters, 357-358, 99-110.
497 Griffin, W.L., Fisher, N.I., Friedman, J.H., O'Reilly, S.Y., and Ryan, C.G. (2002) Cr-pyrope garnets in
498 the lithospheric mantle. II. Compositional populations and their distribution in time and space.
499 Geochemistry, Geophysics, Geosystems, 3, 1073, doi:10.1029/2002GC000298.
500 Griffin, W.L., Kaminsky, F.V., Ryan, C.G., O'Reilly, S.Y., Win, T.T., and Ilupin, I.P. (1996) Thermal
501 state and composition of the lithospheric mantle beneath the Daldyn kimberlite field, Yakutia.
502 Tectonophysics, 262, 19-33.
503 Griffin, W.L., O'Reilly, S.Y., Doyle, B.J., Pearson, N.J., Coopersmith, H., Kivi, K., Malkovets, V., and
504 Pokhilenko, N. (2004) Lithosphere mapping beneath the North American plate. Lithos, 77, 873-922.
505 Griffin, W.L., Ryan, C.G., Kaminsky, F.V., O'Reilly, S.Y., Natapov, L.M., Win, T.T., Kinny, P.D.,
506 and Ilupin, I.P. (1999) The Siberian lithosphere traverse. Mantle terranes and the assembly of the
507 Siberian craton. Tectonophysics, 310, 1-35.
508 Grütter, H., Latti, D., and Menzies, A.H. (2006) Cr-saturation arrays in concentrate garnet
509 compositions from kimberlite and their use in mantle barometry. Journal of Petrology, 47, 801-820.
510 Grütter, H., and Moore, R. (2003) Pyroxene geotherms revisited - an empirical approach based on
511 Canadian xenoliths. Extended Abstract 8th International Kimberlite Conference no. 272.
512 Grütter, H.S. (2009) Pyroxene xenocryst geotherms: techniques and application. Lithos, 112, 1167-
513 1178.
514 Grütter, H.S., and Tuer, J. (2009) Constraints on deep mantle tenor of Sarfartoq-area kimberlites
515 (Greenland), based on modern thermobarometry of mantle-derived xenocrysts. Lithos, 112, 124-
516 129.
517 Hasterok, D., and Chapman, D.S. (2011) Heat production and geotherms for the continental
518 lithosphere. Earth and Planetary Science Letters, 307, 59-70.

519 Ionov, D.A., Doucet, L.S., and Ashchepkov, I.V. (2010) Composition of the lithospheric mantle in the
520 Siberian craton: new constraints from fresh peridotites in the Udachnaya-East kimberlite. Journal of
521 Petrology, 51, 2177-2210.
522 Janney, P.E., Shirey, S.B., Carlson, R.W., Pearson, D.G., Bell, D.R., Le Roex, A.P., Ishikawa, A.,
523 Nixon, P.H., and Boyd, F.R. (2010) Age, composition and thermal characteristics of South African
524 off-craton mantle lithosphere: Evidence for a multi-stage history. Journal of Petrology, 51, 1849-
525 1890.
526 Kopylova, M.G., Russell, J.K., and Cookenboo, H. (1998) Upper-mantle stratigraphy of the Slave
527 craton, Canada: Insights into a new kimberlite province. Geology, 26, 315-318.
528 Lazarov, M., Woodland, A.B., and Brey, G.P. (2009) Thermal state and redox conditions of the
529 Kaapvaal mantle: A study of xenoliths from the Finsch mine, South Africa. Lithos, 112S, 913-923.
530 Lehtonen, M., O'Brien, H., Peltonen, P., Kukkonen, I., Ustinov, V., and Verzhak, V. (2009) Mantle
531 xenocrysts from the Arkhangelskaya kimberlite (Lomonosov mine, NW Russia): Constraints on the
532 composition and thermal state of the diamondiferous lithospheric mantle. Lithos, 112, 924-933.
533 Lepekhina, E.N., Rotman, A.Y., Antonov, A.V., and Sergeev, S.A. (2008a) SHRIMP U-Pb zircon of
534 Yakutian kimberlites pipes. Extended Abstract 9th International Kimberlite Conference, no. 9IKC-
535 A-00354.
536 Lepekhina, E.N., Rotman, A.Y., Antonov, A.V., and Sergeev, S.A. (2008b) SHRIMP U-Pb perovskite
537 from kimberlites of the Siberian platform (Verhnemunskoe and Alakite-Marhinskoe fields).
538 Extended Abstract 9th International Kimberlite Conference, no. 9IKC-A-00353.
539 Levchenkov., O.A., Gaidamako, I.M., Levskii, L.K., Komarov, A.N., Yakovleva, S.Z., Rizvanova
540 N.G., and Makeev, A.F. (2005) U-Pb age of zircon from the Mir and 325 Let Yakutii Pipes.
541 Doklady Earth Science, 400, 99-101.
542 Malkovets, V.G., Griffin, W.L., O'Reilly, S.Y., and Wood, B.J., 2007. Diamond, subcalcic garnet, and
543 mantle metasomatism: kimberlite sampling patterns define the link. Geology 35 (4), 339–342.

544 Manakov, A. (2002) Moho depth beneath the Siberian kimberlite fields. Mirny, Russia. 352 p. PhD
545 thesis.
546 Mather, K.A., Pearson, D.G., McKenzie, D., Kjarsgaard, B.A., and Priestley, K. (2011) Constraints on
547 the depth and thermal history of cratonic lithosphere from peridotite xenoliths, xenocrysts and
548 seismology. Lithos, 125, 729-742.
549 McKenzie, D., and Bickle, M.J. (1988) The volume and composition of melt generated by extension of
550 the lithosphere. Journal of Petrology, 29, 625-679.
551 McKenzie, D., Jackson, J., and Priestley, K. (2005) Thermal structure of oceanic and continental
552 lithosphere. Earth and Planetary Science Letters, 233, 337-349.
553 Menzies, A., Westerlund, K., Grütter, H., Gurney, J., Carlson, J., Fung, A., and Nowicki, T. (2004)
554 Peridotitic mantle xenoliths from kimberlites on the Ekati Diamond Mine property, N.W.T., Canada:
555 major element compositions and implications for the lithosphere beneath the central Slave craton.
556 Lithos, 77, 395-412. Chemical Geology, 368, 97-103.
557 Nickel, K.G., and Green, D.H. (1985) Empirical geothermobarometry for garnet peridotites and
558 implications for the nature of the lithosphere, kimberlites and diamonds. Earth and Planetary
559 Science Letters, 73, 158-170.
560 Nielsen, C.H., and Sigurdsson, H. (1981) Quantitative methods for electron microprobe analysis of
561 sodium in natural and synthetic glasses. American Mineralogist, 66, 547-552.
562 Nimis, P. (1998) Evaluation of diamond potential from the composition of peridotitic chromian
563 diopside. European Journal of Mineralogy, 10, 505-519.
564 Nimis, P. (2002) The pressures and temperatures of formation of diamond based on thermobarometry
565 of chromian diopside inclusions. Canadian Mineralogist, 40, 871-884.
566 Nimis, P., and Grütter, H. (2010) Internally consistent geothermometers for garnet peridotites and
567 pyroxenites. Contributions to Mineralogy and Petrology, 159, 411-427.

568 Nimis, P., and Taylor, W.R. (2000) Single-clinopyroxene thermobarometry for garnet peridotites. Part
569 I. Calibration and testing of a Cr-in-Cpx barometer and an enstatite-in-Cpx thermometer.
570 Contributions to Mineralogy and Petrology, 139, 541-554.
571 Nimis, P., Zanetti, A., Dencker, I., and Sobolev, N.V. (2009) Major and trace element composition of
572 chromian diopsides from the Zagadochnaya kimberlite (Yakutia, Russia): Metasomatic processes,
573 thermobarometry and diamond potential. Lithos, 112, 397-412.
574 O'Reilly, S.Y., and Griffin, W.L. (1985) A xenolith-derived geotherm for southeastern Australia and its
575 geological implications. Tectonophysics, 111, 41-63.
576 Osako, M., Ito, E., and Yoneda, A. (2004) Simultaneous measurements of thermal conductivity and
577 thermal diffusivity for garnet and olivine under high pressure. Physics of the Earth and Planetary
578 Interiors, 143, 311-320.
579 Pokhilenko, N.P., Sobolev, N.V., Boyd, F.R., Pearson, D.G., and Shimuzu, N. (1993) Megacrystalline
580 pyrope peridotites in the lithosphere of the Siberian platform: Mineralogy, geochemical peculiarities
581 and the problem of their origin. Russian Geology and Geophysics, 34, 56-67.
582 Pokhilenko, N.P., Sobolev, N.V., Kuligin, S.S., and Shimizu, N. (1999) Peculiarities of distribution of
583 pyroxenite paragenesis garnets in Yakutian kimberlites and some aspects of the evolution of the
584 Siberian craton lithospheric mantle. In: J.J. Gurney, J.L. Gurney, M.D. Pascoe, S.H. Richardson
585 (Eds.), Proceedings of the 7th International Kimberlite Conference, vol.2. p. 689-698.
586 Pollack, H.N., and Chapman, D.S. (1977) On the regional variations of heat flow, geotherms and
587 lithospheric thickness. Tectonophysics, 38, 279-296.
588 Potts, P.J., Tindle A.G., and Isaacs, M.C. (1983) On the precision of electron microprobe data: a new
589 test for the homogeneity of mineral standards. American Mineralogist, 68, 1237-1242.
590 Putirka, K.D. (2008) Thermometers and barometers for volcanic systems. Reviews in Mineralogy and
591 Geochemistry, 69, 61-120.

592 Ramsay, R.R., and Tompkins, L.A. (1994) The geology, heavy mineral concentrate mineralogy, and
593 diamond prospectivity of the Boa Esperança and Cana Verde pipes, Corrego D'anta, Minas Gerais,
594 Brazil. In: H.O.A. Meyer, O.H. Leonardos (Eds.), Kimberlites, Related Rocks and Mantle Xenoliths
595 CPRM, Special Publications, p. 329-345, Brasilia, Brazil.
596 Read, G.H., and Janse, A.J.A. (2009) Diamonds: Exploration, mines and marketing. Lithos, 112, 1-9.
597 Read, G.H., Grütter, H., Winter, S., Luckman, N., Gaunt, F., and Thomsen, F. (2004) Stratigraphic
598 relations, kimberlite emplacement and lithospheric thermal evolution, Quirico´ Basin, Minas Gerais
599 State, Brazil. Lithos, 77, 803–818.
600 Rosen, O.M., Soloviev, A.V., and Zhuravlev, D.Z. (2009) Thermal evolution of the northeastern
601 Siberian Platform in the light of apatite fission-track dating of the Deep Drill Core. Izvestiya,
602 Physics of the Solid Earth, 45, 914-931.
603 Ryan, C.G., Griffin, W.L., and Pearson, N.J. (1996) Garnet geotherms: pressure–temperature data from
604 Cr-pyrope garnet xenocrysts in volcanic rocks. Journal of Geophysical Research, 101, 5611-5625.
605 Shimizu, N., Pokhilenko, N.P., Boyd, F.R., and Pearson, D.G. (1997) Geochemical characteristics of
606 mantle xenoliths from the Udachnaya kimberlite pipe. Proceedings of the 6th International
607 Kimberlite Conference vol.1, p. 205-217.
608 Shirey, S.B., Cartigny, P., Frost, D.J., Keshav, S., Nestola, F., Nimis, P., Pearson, D.G., Sobolev, N.V.,
609 and Walter, M.J. (2013) Diamonds and the geology of mantle carbon. Reviews in Mineralogy and
610 Geochemistry, 75, 355-421.
611 Smith, D. (1999) Temperatures and pressures of mineral equilibration in peridotite xenoliths: review,
612 discussion, and implications. In: Y. Fei, C.M. Bertka, B.O. Mysen (Eds.), Mantle petrology: field
613 observations and high pressure experimentation: a tribute to Francis R. (Joe) Boyd, vol 6.
614 Geochemical Society Special Publications, p. 171-188.
615 Stachel, T., and Harris, J.W. (2008) The origin of cratonic diamonds – constraints from mineral
616 inclusions. Ore Geology Review, 34, 5-32.

Sun, J., Liu, C.Z., Tappe, S., Kostrovitsky, S.I., Wu, F.Y., Yakovlev, D., Yang, Y.-H., and Yang, J.H. (2014) Repeated kimberlite magmatism beneath Yakutia and its relationship to Siberian flood volcanism: insights from in situ U–Pb and Sr–Nd perovskite isotope analysis. Earth Planet. Sci. Lett. 404, 283-295.

Taylor, W.R. (1998) An experimental test of some geothermometer and geobarometer formulations for upper mantle peridotites with application to the thermobarometry of fertile lherzolite and garnet websterite. Neues Jahrbuch für Mineralogie, Abhandlungen, 172, 381-408.

Wang, W., and Gasparik, T. (2001) Metasomatic clinopyroxene inclusions in diamonds from the Liaoning province, China. Geochimica et Cosmochimica Acta, 65, 611-62.

Zozulya, D.R., O'Brien, H., Peltonen, P., and Lehtonen, M. (2009) Thermobarometry of mantle-derived garnets and pyroxenes of Kola region (NW Russia): Lithosphere composition, thermal regime and diamond prospectivity. Bulletin of the Geological Society of Finland, 81, 143-15.

APPENDIX. PROPAGATION OF ANALYTICAL ERRORS IN SINGLE-CLINOPYROXENE GEOBAROMETRY

The Cr-in-Cpx barometer (Nimis and Taylor, 2000) is expressed as

$$P(\text{kbar}) = -\frac{T(\text{K})}{126.9} \cdot \ln a_{\text{Cr}} + 15.483 \cdot \ln\left(\frac{Cr\#}{T(\text{K})}\right) + \frac{T(\text{K})}{71.38} + 107.8 \qquad (1)$$

where a_{Cr} = Cr – 0.81·Na·*Cr*# and *Cr*# = Cr/(Cr+Al), with elements in apfu. Although the effect of K on Cpx barometry was unknown, Nimis and Taylor (2000) suggested that any K should be added to Na in *P* calculations. Assuming random error sources, the uncertainties on pressure estimates can be expressed with a normal error propagation function, i.e.,

$$\sigma P = \sqrt{\left(\frac{\partial P}{\partial \text{Cr}} \cdot \sigma\text{Cr}\right)^2 + \left(\frac{\partial P}{\partial \text{Al}} \cdot \sigma\text{Al}\right)^2 + \left(\frac{\partial P}{\partial \text{Na}} \cdot \sigma\text{Na}\right)^2 + \left(\frac{\partial P}{\partial T} \cdot \sigma T\right)^2} \qquad (2)$$

Calculation of σP requires knowledge of analytical uncertainties on Cr, Al, Na and *T*. The influence of analytical uncertainties on the very minor K contents can safely be neglected. Uncertainties on *T* estimates can be derived from reproducibility of temperatures of experiments in two-pyroxene-bearing assemblages using the enstatite-in-Cpx thermometer (±30–40°C; Nimis and Taylor 2000). Accurate evaluation of EMP uncertainties is not straightforward, because analytical errors primarily depend on both the absolute element concentrations and on the analytical conditions adopted for the analysis.

In this appendix, we will investigate the effect of EMP uncertainties on pressure estimates for compositionally diverse clinopyroxenes. As a first step, we will evaluate the analytical errors for different analytical conditions and for a specific set of clinopyroxene compositions through repeat EMP measurements on compositionally homogeneous areas of selected cpx grains, and evaluate the propagated uncertainties on *P* estimates by calculating *P* for each analysis. We then apply the error propagation function (Equation 2) to a great variety of natural clinopyroxene compositions, assuming model analytical uncertainties derived from the first test.

First step: evaluation of uncertainties vs. analytical conditions

655 We selected seven clinopyroxenes having a_{Cr} between 0.0016 and 0.0188 apfu, characterized by
656 various proportions of Al, Cr and Na, and equilibrated in a wide range of *P–T* conditions (Table A1).
657 Appropriate compositions were found in four clinopyroxene xenocrysts from the Novinka kimberlite
658 (this study) and three clinopyroxenes from three well-studied garnet peridotites. Description of the
659 garnet peridotite samples is reported in Supplementary Material S3.
660 Chemical analyses were carried out with a CAMECA SX-50 electron microprobe (IGG–CNR,
661 Padua, Italy), equipped with four wavelength-dispersive spectrometers using one LIF, one PET, and
662 two TAP crystals. Natural and synthetic minerals (diopside for Ca and Si, albite for Na, orthoclase for
663 K, and pure Al, Mg, Cr, Fe, and Mn-Ti oxides) were used as standards. X-ray counts were converted
664 into weight percent oxides by using the CAMECA-PAP program. Each clinopyroxene grain/portion
665 was first analyzed for all elements adopting routine analytical condition, i.e., 1 μm electron beam, 20
666 kV accelerating voltage, 15 nA beam current, and a counting time of 10 s for peak and 10 s for
667 background (i.e., 5 s on each side of the peak). The most mobile elements were always analyzed first in
668 order to minimize their migration under the electron beam. The sequence of element analyses on each
669 spectrometer was thus as follows: Fe, Mn, Cr (LIF); Si, Al (TAP); Na, Mg (TAP); K, Ca, Ti (PET).
670 This preliminary investigation allowed us to select compositionally homogeneous areas and provided
671 us with average compositions to be used for calculation of matrix effects in subsequent analytical
672 sessions and for preliminary thermobarometry (Table A1).
673 The same clinopyroxenes were then analyzed again for Al, Cr and Na using increasing beam
674 currents and counting times (Table A2). Five analytical sessions were carried out, during which 15
675 individual point analyses were acquired on the same, homogeneous areas of each clinopyroxene. The
676 analyses were carried out on a grid of 3 x 5 analytical spots (maximum side 20 μm). To limit element
677 migration under the electron beam, before each session the grid was translated by 3–4 μm, within the
678 previously defined homogeneous areas. Calcium was also measured on the same spots as a further
679 check for compositional homogeneity. The four elements were analyzed simultaneously with the four

680 independent spectrometers. Observed absolute variations in CaO weight percentages between
681 individual point analyses were always ≤0.5 wt%. No systematic variations in X-ray counts for Na were
682 observed using different beam currents (i.e., 15 nA and 40 nA), not even after a 300-s count period,
683 implying that Na did not significantly mobilize under the electron beam during our analyses (cf.
684 Nielsen and Sigurdsson 1981). No analyses for which any measured concentration departed by more
685 than 3 standard deviations from the mean were obtained. The average compositions obtained during the
686 five test sessions on each selected clinopyroxene are reported in Table A3.
687 For each point analysis, *Cr#*, a_{Cr} and Cr-in-Cpx pressure were calculated. Pressures were calculated
688 using fixed input temperature values, which were obtained by applying the enstatite-in-Cpx
689 thermometer, at *P* given by the Cr-in-Cpx barometer, on the compositions derived from the preliminary
690 analyses of the samples (Table A1). Statistical parameters (mean values, standard deviations, and
691 quantiles) for all relevant variables are reported in Table A3 and illustrated in Figure A1.
692 The relative uncertainties on the measured Al, Cr and Na concentrations decrease smoothly with
693 increasing beam current, counting times, and element abundances (Table A3). This allowed us to
694 model analytical uncertainties as functions of clinopyroxene composition for each set of analytical
695 conditions (Table A4). The standard deviations on *P* estimates drastically change with changing
696 analytical conditions (σ as high as 1.1 GPa using the lowest beam current and counting times) and
697 clinopyroxene composition (Table A3 and Fig. A1).
698 The relationships between *P* uncertainties and composition can be explained considering the
699 topology of the Cr-in-Cpx barometer expression (Equation 1). In equation (1), *P* is related to a_{Cr} and
700 *Cr#* through two logarithmic functions. This enhances error propagation with decreasing a_{Cr} and *Cr#*.
701 Owing to its greater weight in the equation, the effect of the a_{Cr} logarithmic term tends to be dominant
702 in terms of error propagation. This accounts well for the larger *P* uncertainties obtained for the
703 clinopyroxene Nov-42 (a_{Cr} = 0.0016 apfu) with respect to clinopyroxene Uv61/91 (a_{Cr} = 0.0081 apfu),
704 in spite of their similar a_{Cr} uncertainties (Table A3). It also explains the progressively larger, non-

systematic deviations from orthopyroxene–garnet pressures at lower a_{Cr} (Figs. 2 and 4). Moreover, because of the logarithmic relation, the distribution of propagated errors due to a_{Cr} uncertainties tends to be skewed towards the positive side.

Whereas the effect of the *Cr#* logarithmic term on error propagation is marginal, *Cr#* has a major effect on the uncertainties of the a_{Cr} parameter. In particular, a higher *Cr#* will enhance propagation of Na uncertainties on a_{Cr} and, therefore, on *P*. This explains the lower *P* uncertainties (and their less pronounced variations between different analytical sessions) obtained for clinopyroxene Nov-80, which is characterized by low a_{Cr} (0.003 apfu) *and* low *Cr#* (0.13), compared with those obtained for compositions with higher *Cr#* values (Table A3 and Fig. A1).

Second step: *P* uncertainties in the natural clinopyroxene compositional space and optimum analytical conditions for clinopyroxene barometry

The above test showed that the effect of analytical errors on the precision and accuracy of the calculated pressure strongly increases with decreasing a_{Cr} and with increasing *Cr#*. For any clinopyroxene composition, minimum analytical conditions should be defined for which analytical errors propagate acceptable errors on pressure estimates. For this purpose, a more extended test on a comprehensive set of clinopyroxene compositions is needed. We have used the database of well-equilibrated xenoliths of Nimis and Grütter (2010) as our test material. Temperatures for each xenolith were calculated using the thermometer of Taylor (1998) at *P* given by the orthopyroxene–garnet barometer of Nickel and Green (1985; with modifications by Carswell 1991, his equations E6 and E9, assuming no ferric iron). The *T* uncertainty was fixed at 40 °C (cf. Nimis and Taylor 2000). Uncertainties on clinopyroxene Cr, Al and Na analyses were calculated for each xenolith for five combinations of analytical conditions, taking into account the results of our previous analytical test (Table A4). Uncertainties on Cr-in-Cpx pressures were then calculated by normal error propagation of the five resulting sets of analytical uncertainties (Equation 2).

As expected, the calculated uncertainties increase with decreasing a_{Cr} and increasing *Cr#* values (Fig. 3), reaching 1.8 GPa when a_{Cr} is <0.002 apfu and the lowest current and counting times are assumed. These results can be used to determine an approximate compositional threshold below which pressure estimates become too sensitive to analytical errors. We consider a propagated uncertainty of ±0.25 GPa on the calculated *P*, including the effect of both analytical and thermometric errors, to be a reasonable limit. Taking into account the standard error of estimate of the barometer calibration (±0.23 GPa), this limit should ensure an overall uncertainty smaller than ±0.4 GPa. We found that simplified thresholds based on the a_{Cr}/*Cr#* ratio (Table A2) permit discrimination of compositions for which *P* uncertainties are acceptable to within a 95% confidence limit.

741 **Figure 1.** Sketch tectonic map of the Siberian platform with major kimberlite fields. Terranes are
742 outlined by dashed curves and are named in italic. Modified after Griffin et al. (1999).
743 **Figure 2.** Discrepancies between the Cr-in-Cpx barometer (Nimis and Taylor 2000; P_{NT00}) and the
744 orthopyroxene-garnet barometer (P_{Ca91}; Nickel and Green 1985, as modified by Carswell 1991) vs. the
745 clinopyroxene parameter a_{Cr}. Clinopyroxene compositions are from the compilation of well-
746 equilibrated garnet peridotite and pyroxenite xenoliths of Nimis and Grütter (2010). In **(a)** the entire
747 dataset has been included, while in **(b)** only clinopyroxene plotting in the high-Al field of Nimis (1998)
748 [$Al_2O_3 \geq 0.7$ wt%; $Al_2O_3 \geq 12.175 - 0.6375$*MgO wt%] and having *Cr#* between 0.06 and 0.50
749 (Grütter, 2009) have been plotted. The overall shift of high-*P* clinopyroxenes towards negative values
750 can be ascribed to the known underestimation of PNT00 at high *P* (cf. Nimis 2002).
751 **Figure 3.** Calculated *P* uncertainties (σ) vs. a_{Cr} for clinopyroxenes from well-equilibrated garnet
752 peridotites and pyroxenites (database of Nimis and Grütter 2010). The *P* uncertainties were calculated
753 from normal propagation of *T* uncertainties (±40°C) and analytical errors derived from equations
754 reported in Table A4 assuming **(a)** the lowest beam current (15 nA) and counting times (10 s peak, 5 +
755 5 s background) and **(b)** the highest beam current (40nA) and counting times (40 s peak, 20 + 20 s
756 background).
757 **Figure 4.** *P* estimates using the Cr-in-Cpx barometer (Nimis and Taylor 2000; P_{NT00}) plotted versus *P*
758 estimates using the orthopyroxene–garnet barometer of Nickel and Green (1985, as modified by
759 Carswell 1991; P_{Ca91}) for **(a)** the entire dataset of well equilibrated garnet peridotites and pyroxenites of
760 Nimis and Grütter (2010) and **(b)** the same dataset excluding samples with calculated Cr-in-Cpx
761 pressure uncertainties greater than ±0.25 GPa.
762 **Figure 5.** Results of single-clinopyroxene thermobarometry (Nimis and Taylor 2000) for the Novinka
763 kimberlite. In **(a)** the accepted analyses have been selected on the basis of the revised protocol for
764 single-clinopyroxene thermobarometry (this work), which takes into account the results of our
765 analytical test (Appendix). For comparison, plot **(b)** shows the results of the filtering protocol of

766 Grütter (2009) applied on the same initial dataset (97 routine analyses; see text). Dashed curves are
767 classical reference conductive geotherms for different surface heat-flows (mW/m^2) after Pollack and
768 Chapman (1977). The graphite (G) - diamond (D) boundary (solid curve) is after Day (2012).
769 **Figure 6.** Model palaeogeotherms calculated using the program FITPLOT (McKenzie et al. 2005). The
770 palaeogeotherm for Novinka are calculated **(a)** using all *P–T* estimates based on optimized
771 clinopyroxene analyses and **(b)** excluding data plotting above 5.5 GPa. The smaller plots show *P–T*
772 data for Udachnaya xenoliths, calculated using the geothermometer of Nimis and Taylor (2000; T_{NT00})
773 in combination with **(c)** the Nickel and Green (1985; P_{NG85}) geobarometer, **(d)** its modification by
774 Carswell (1991; P_{Ca91}), and **(e)** the Cr-in-Cpx geobarometer of Nimis and Taylor (2000; P_{NT00}). Grey
775 symbols in **(e)** indicate clinopyroxenes for which the calculated σ_P is > 0.25 GPa (taking into account
776 the analytical conditions used for the analysis as reported in the source papers). Source mineral
777 compositions for Udachnaya are from Boyd (1984), Pokhilenko et al. (1993), Shimizu et al. (1997),
778 Ionov et al. (2010), Goncharov et al. (2012), and Doucet et al. (2013).
779 **Figure 7**. Relationships between *P*/*T* gradients, a_{Cr}/*Cr#* in clinopyroxene, and uncertainties of Cr-in-
780 Cpx pressure propagated from analytical errors. Filled circles are a_{Cr}/*Cr#* values of the experimental
781 clinopyroxenes used for the calibration of the Cr-in-Cpx barometer (Nimis and Taylor 2000), empty
782 squares are a_{Cr}/*Cr#* values of natural clinopyroxenes from well-equilibrated peridotites (Nimis and
783 Grütter 2010) and crosses are calculated *P* uncertainties for the same dataset (see Fig. 3 and text for
784 calculation methods). Natural clinopyroxenes with *Cr#* < 0.1, which are considered usnsuitable for
785 geobarometry (see text), were excluded from the plot. The approximate correspondence between *P*/*T*
786 gradients and steady-state continental geotherms (Pollack and Chapman 1977) is also indicated at the
787 top of the plot. Geobarometry of clinopyroxenes from relatively cold mantle sections (< 40 mW/m^2) is
788 clearly more sensitive to propagation of analytical errors.
789

790 **Figure A1.** Box-plots of calculated pressures for the test clinopyroxenes analyzed using different
791 operating conditions (cf. Table A2). Median values (thicker vertical lines), interquartile range (boxes),
792 whiskers (dashed lines indicating variability outside the upper and lower quartiles) and individual *P*
793 estimates for each point analyses (empty circles) are shown. A few analyses of sample Nov-42 resulted
794 in negative values of a_{Cr} and were therefore excluded from calculations.
795

Figure 1

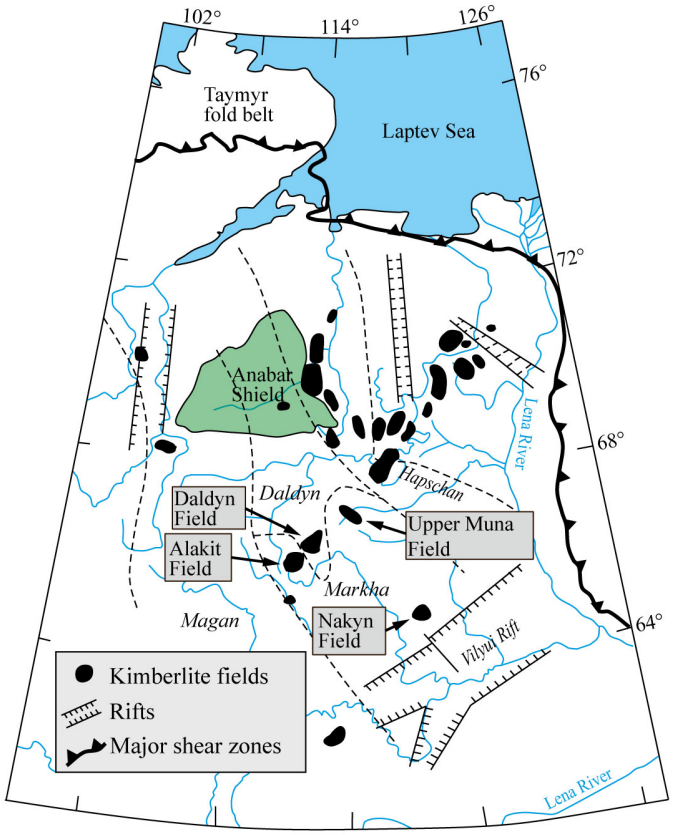
102°
114°
126°
76°
72°
68°
64°
Taymyr
fold belt
Laptev Sea
Anabar
Shield
Lena River
Daldyn
Daldyn
Field
Alakit
Field
Hapschan
Upper Muna
Field
Markha
Magan
Nakyn
Field
Vilyui Rift
Kimberlite fields
Rifts
Major shear zones
Lena River

Figure 2

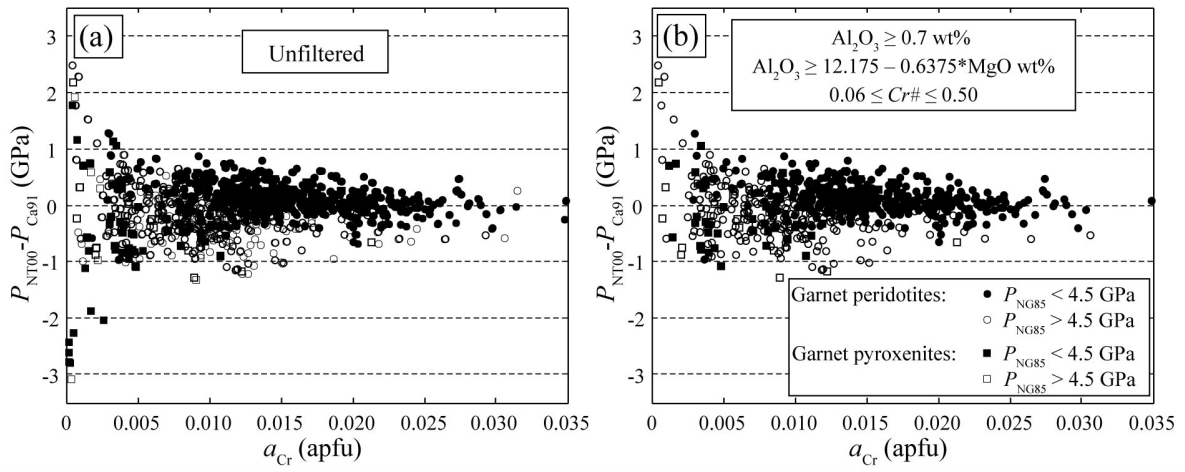

Figure 3

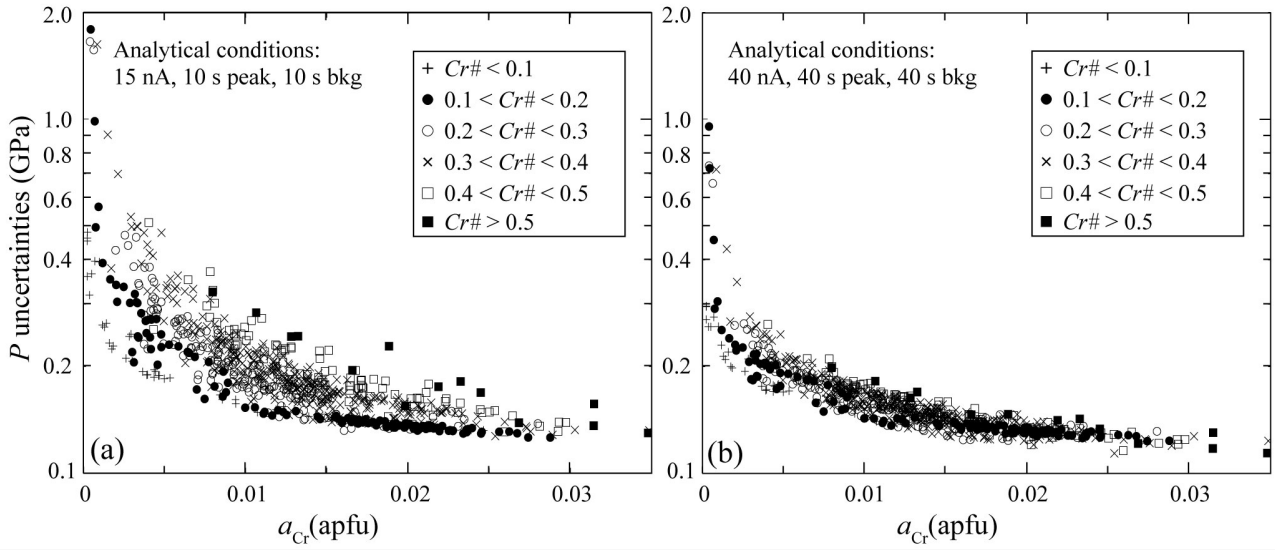

Figure 4

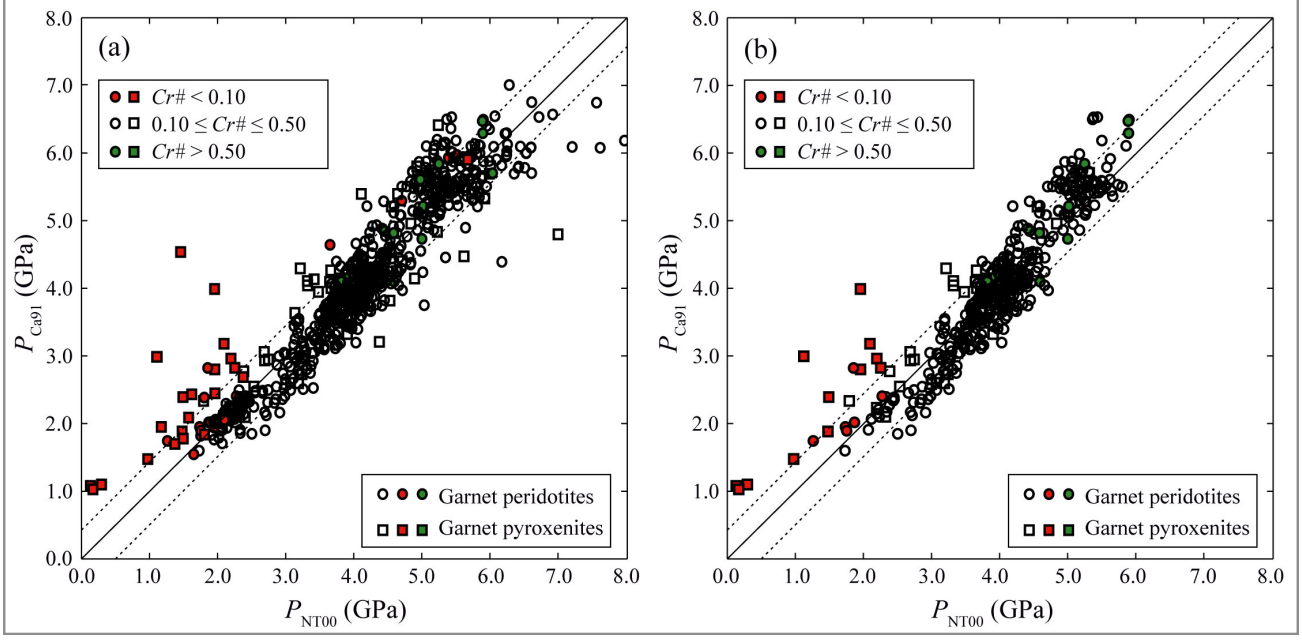

Figure 5

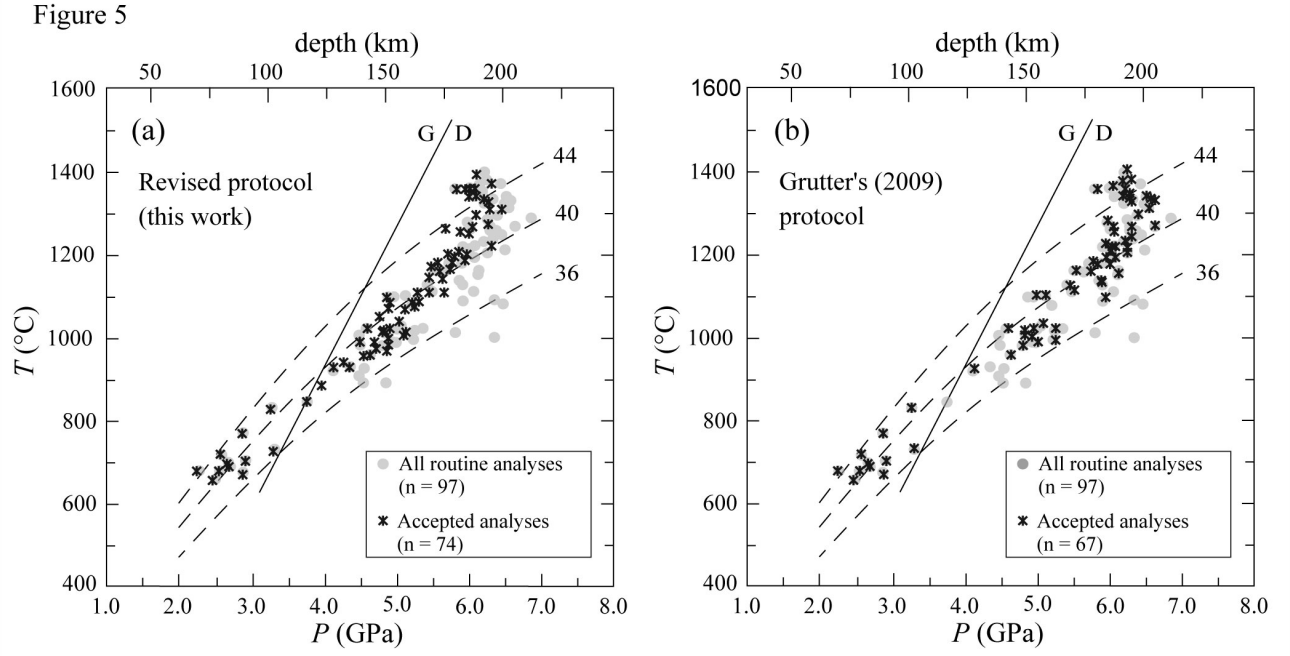

Figure 6

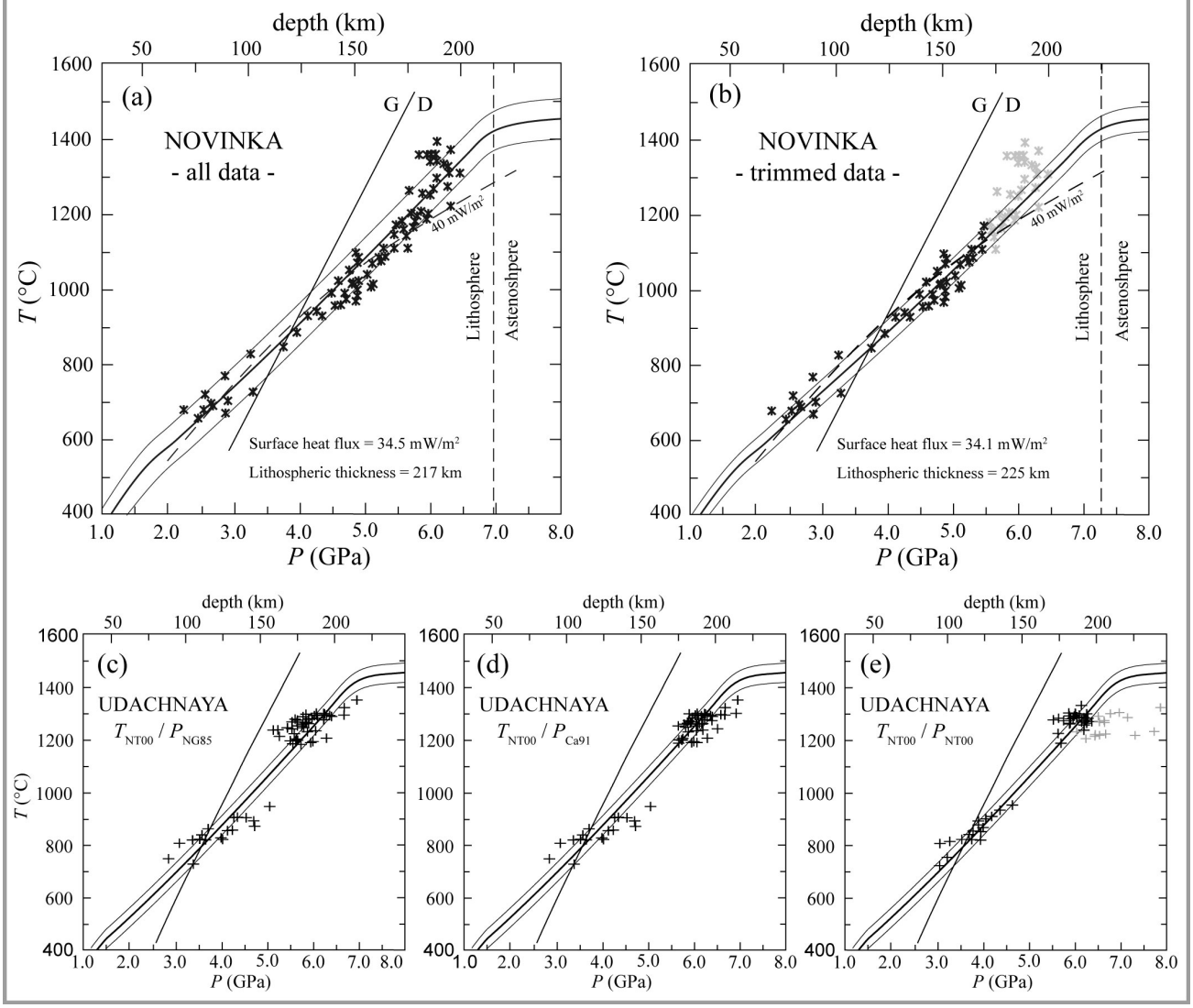
depth (km)
50
100
150
200
(a)
NOVINKA
- all data -
G
D
40 mW/m²
Lithosphere
Astenoshpere
Surface heat flux = 34.5 mW/m²
Lithospheric thickness = 217 km
T (°C)
P (GPa)
(b)
NOVINKA
- trimmed data -
Surface heat flux = 34.1 mW/m²
Lithospheric thickness = 225 km
(c)
UDACHNAYA
T_{NT00} / P_{NG85}
(d)
UDACHNAYA
T_{NT00} / P_{Ca91}
(e)
UDACHNAYA
T_{NT00} / P_{NT00}

Figure 7

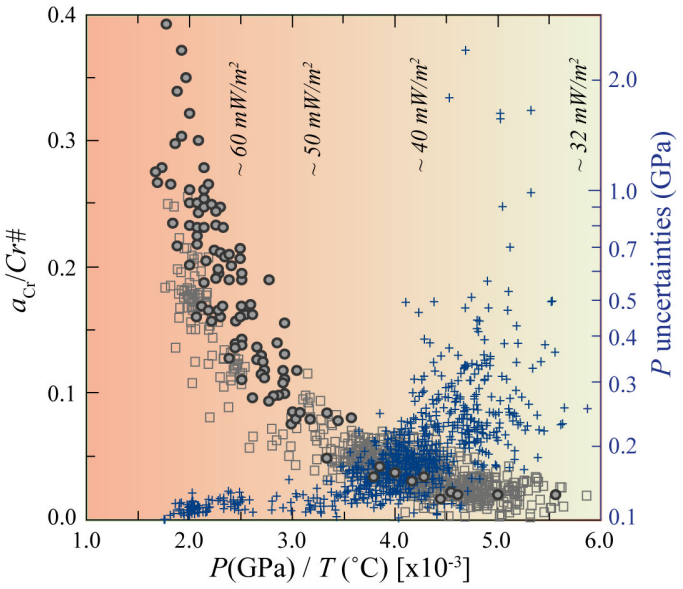
0.4
0.3
0.2
0.1
0.0
a_{Cr}/Cr#
~ 60 mW/m²
~ 50 mW/m²
~ 40 mW/m²
~ 32 mW/m²
2.0
1.0
0.7
0.5
0.4
0.3
0.2
0.1
P uncertainties (GPa)
1.0
2.0
3.0
4.0
5.0
6.0
P(GPa) / T (°C) [x10⁻³]

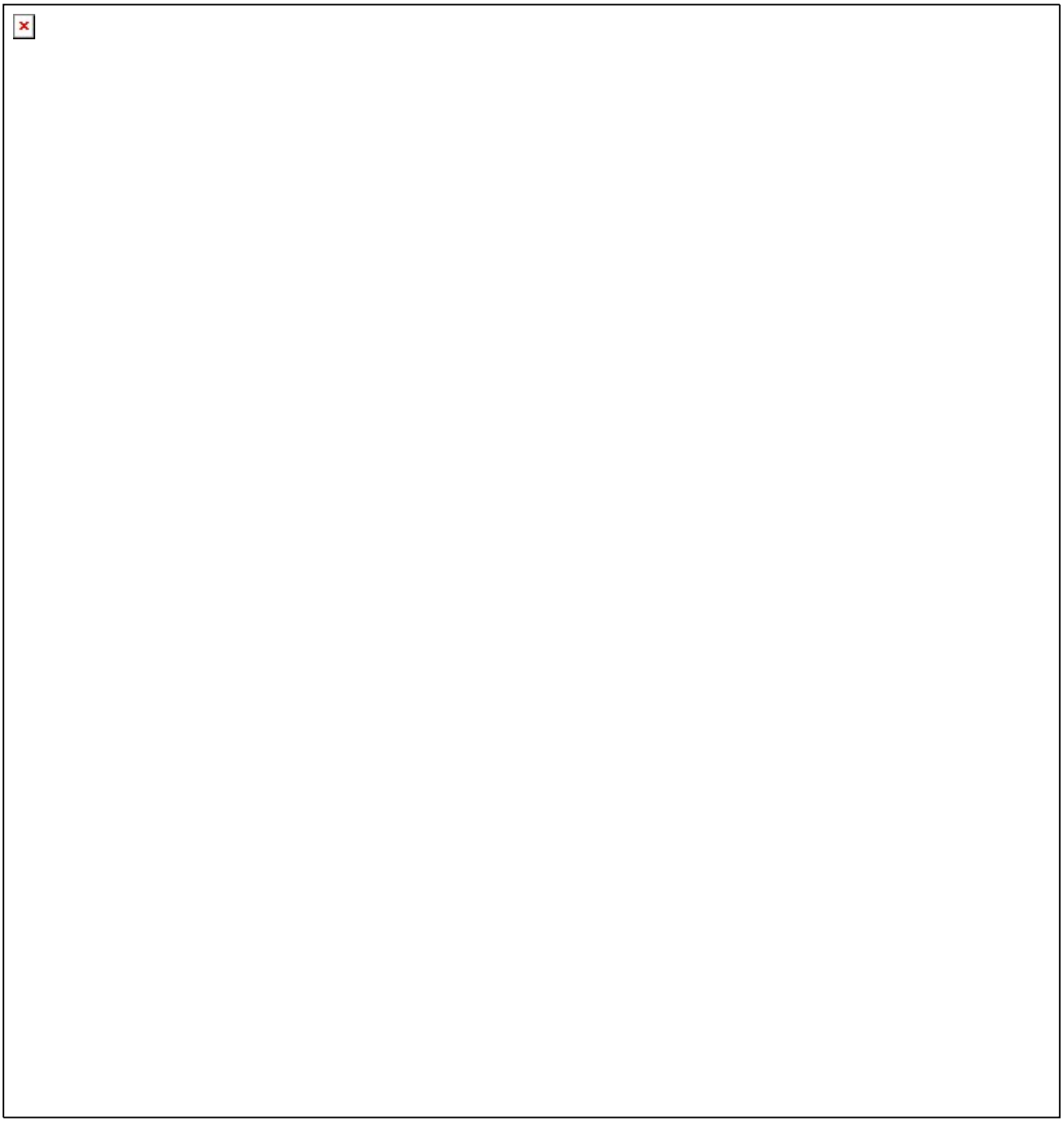

Table A1. Compositions (15 nA, 20 kV, 10 s peak + 10 s background) of clinopyroxenes used for the evaluation of propagation of analytical errors.

Sample	Nov-42	Nov-69	Nov-80	Nov-114	FRB1031	KGG-65	Uv61/91
SiO_2	54.82	54.32	55.08	54.65	55.69	54.57	54.88
TiO_2	0.27	0.24	0.21	0.30	0.25	0.28	0.05
Al_2O_3	2.21	2.06	2.46	1.77	2.46	2.65	0.61
Cr_2O_3	1.17	2.42	0.61	1.28	1.32	2.4	0.94
FeO_{tot}	3.83	3.14	4.39	4.01	3.26	2.26	2.45
MnO	0.12	0.11	0.09	0.11	0.11	0.06	0.10
MgO	16.30	15.95	20.20	18.27	19.23	16.15	19.20
CaO	18.58	18.57	14.58	17.07	16.74	19.5	20.92
Na_2O	2.12	2.34	1.85	1.74	1.89	2.32	0.65
K_2O	0.04	0.03	0.03	0.04	0.03	< 0.02	< 0.02
Sum	99.47	99.18	99.51	99.23	100.95	100.19	99.80
Cr#	0.27	0.44	0.14	0.33	0.27	0.39	0.51
a_{Cr}	0.0016	0.0103	0.0023	0.0037	0.0092	0.0188	0.0081
T_{NT00} (°C)	1088	1006	1369	1265	1270	912	1180
P_{NT00} (GPa)	6.32	4.84	6.44	6.61	5.22	3.69	6.01
T_{Ta98} (°C)	-	-	-	-	1265	972	1190
P_{Ca91} (GPa)	-	-	-	-	5.62	3.84	6.09

NT00 – Nimis and Taylor (2000); Ta98 – Taylor (1998); Ca91 – Nickel and Green (1985) with modifications by Carswell (1991). T_{Ta98} and P_{Ca91} for source xenoliths calculated using orthopyroxene and garnet compositions after Boyd (personal communication), Canil and O'Neill (1996) and Franz et al. (1996) and clinopyroxene compositions reported here.

Table A2. Electron microprobe operating conditions for the different analytical sessions. Accelerating voltage was fixed to 20 kV. The last row indicates the minimum $a_{Cr}/Cr\#$ values required to maintain the propagated pressure uncertainties within ±0.25 GPa (1σ) (see section 2 of the Appendix).

Session	15-10/10	15-20/20	15-40/40	40-10/10	40-20/20	40-40/40
Beam current (nA)	15	15	15	40	40	40
Peak (sec)	10	20	40	10	20	40
Background (sec)	5 + 5	10 + 10	20+20	5 + 5	10 + 10	20 + 20
$a_{Cr}/Cr\#$	0.024	0.018	0.015	0.018	0.013	0.011

Table A3. Results of analytical sessions on selected clinopyroxenes using different operating condition (cf. Table A2).

Sample	AC	N	CaO		Al_2O_3		Cr_2O_3		Na_2O		*Cr#*		a_{Cr}		*P*	
			av	1σ	av	1σ	av	1σ	av	1σ	av	1σ	av	1σ	av	1σ
Nov-42	1510	15*	18.86	0.12	2.23	0.05	1.12	0.05	2.21	0.06	0.25	0.01	0.0001	0.0012	7.15	1.07
	1520	15*	18.84	0.08	2.24	0.02	1.14	0.04	2.19	0.03	0.25	0.01	0.0006	0.0005	7.37	1.04
	1540	15	18.87	0.06	2.25	0.02	1.12	0.04	2.17	0.02	0.25	0.01	0.0008	0.0005	7.18	0.70
	4010	15	18.81	0.05	2.23	0.03	1.14	0.04	2.18	0.04	0.25	0.01	0.0005	0.0008	7.30	1.01
	4020	15	18.94	0.03	2.25	0.02	1.12	0.03	2.18	0.02	0.25	0.00	0.0006	0.0004	7.42	0.72
	4040	15	18.85	0.05	2.24	0.02	1.14	0.01	2.18	0.02	0.25	0.00	0.0008	0.0002	7.06	0.34
Nov-69	1510	15	18.88	0.10	2.06	0.04	2.32	0.09	2.38	0.07	0.43	0.01	0.0078	0.0023	5.12	0.33
	1520	15	18.77	0.10	2.05	0.03	2.39	0.04	2.36	0.04	0.44	0.01	0.0090	0.0013	4.97	0.16
	1540	15	18.76	0.06	2.06	0.02	2.36	0.04	2.38	0.03	0.43	0.00	0.0084	0.0007	5.02	0.10
	4010	15	18.72	0.07	2.06	0.03	2.37	0.04	2.37	0.04	0.44	0.01	0.0087	0.0011	5.00	0.13
	4020	15	18.80	0.06	2.05	0.02	2.41	0.04	2.38	0.02	0.44	0.00	0.0088	0.0007	4.99	0.07
	4040	15	18.70	0.03	2.07	0.02	2.38	0.04	2.36	0.01	0.44	0.00	0.0092	0.0007	4.93	0.06
Nov-80	1510	15	14.56	0.16	2.56	0.05	0.56	0.05	1.80	0.05	0.13	0.01	0.0027	0.0005	6.07	0.23
	1520	15	14.49	0.05	2.56	0.04	0.57	0.04	1.81	0.02	0.13	0.01	0.0028	0.0003	6.06	0.13
	1540	15	14.47	0.04	2.58	0.02	0.58	0.03	1.82	0.02	0.13	0.01	0.0029	0.0002	6.03	0.08
	4010	15	14.48	0.05	2.57	0.03	0.57	0.03	1.82	0.04	0.13	0.01	0.0028	0.0004	6.08	0.17
	4020	15	14.56	0.04	2.57	0.02	0.58	0.02	1.81	0.02	0.13	0.00	0.0029	0.0003	6.02	0.10
	4040	15	14.55	0.03	2.54	0.02	0.59	0.02	1.83	0.01	0.13	0.00	0.0027	0.0002	6.17	0.08
Nov114	1510	15	17.23	0.13	1.84	0.05	1.16	0.09	1.76	0.04	0.30	0.02	0.0029	0.0012	6.93	0.60
	1520	15	17.06	0.08	1.84	0.03	1.20	0.05	1.77	0.03	0.30	0.01	0.0032	0.0006	6.73	0.24
	1540	15	17.10	0.05	1.84	0.02	1.19	0.03	1.78	0.03	0.30	0.01	0.0031	0.0005	6.76	0.23
	4010	15	17.14	0.08	1.83	0.02	1.22	0.04	1.78	0.03	0.31	0.01	0.0032	0.0009	6.80	0.35
	4020	15	17.21	0.06	1.85	0.02	1.22	0.04	1.79	0.01	0.31	0.01	0.0032	0.0004	6.72	0.13
	4040	15	17.19	0.04	1.82	0.01	1.25	0.02	1.79	0.01	0.32	0.00	0.0034	0.0004	6.71	0.12
KGG65	1510	15	19.48	0.12	2.65	0.04	2.21	0.07	2.31	0.05	0.36	0.01	0.0162	0.0016	3.75	0.08
	1520	15	19.50	0.08	2.65	0.05	2.21	0.07	2.28	0.04	0.36	0.01	0.0167	0.0011	3.72	0.05
	1540	15	19.52	0.05	2.65	0.02	2.19	0.05	2.29	0.03	0.36	0.01	0.0162	0.0008	3.74	0.05
	4010	15	19.51	0.05	2.63	0.02	2.17	0.05	2.31	0.03	0.36	0.01	0.0154	0.0009	3.78	0.05
	4020	15	19.54	0.05	2.63	0.02	2.17	0.04	2.30	0.02	0.36	0.01	0.0155	0.0008	3.78	0.04
	4040	15	19.58	0.04	2.62	0.01	2.16	0.02	2.30	0.02	0.36	0.00	0.0153	0.0004	3.79	0.02

Table A3. Continued

Sample	AC	N	CaO		Al_2O_3		Cr_2O_3		Na_2O		*Cr#*		a_{Cr}		*P*	
			av	1σ	av	1σ	av	1σ	av	1σ	av	1σ	av	1σ	av	1σ
FRB1031	1510	15	16.75	0.11	2.49	0.06	1.25	0.07	1.88	0.03	0.25	0.01	0.0083	0.0010	5.27	0.13
	1520	15	16.64	0.07	2.43	0.03	1.22	0.04	1.88	0.03	0.25	0.01	0.0076	0.0007	5.38	0.10
	1540	15	16.67	0.06	2.44	0.01	1.24	0.04	1.87	0.03	0.26	0.01	0.0081	0.0006	5.32	0.07
	4010	15	16.75	0.06	2.48	0.03	1.20	0.06	1.90	0.02	0.24	0.01	0.0076	0.0007	5.34	0.07
	4020	15	16.77	0.07	2.47	0.02	1.20	0.02	1.89	0.02	0.25	0.00	0.0076	0.0003	5.34	0.04
	4040	15	16.80	0.08	2.48	0.01	1.21	0.02	1.89	0.02	0.25	0.00	0.0076	0.0003	5.33	0.04
Uv6191	1510	15	20.97	0.13	0.61	0.02	0.79	0.05	0.67	0.04	0.47	0.02	0.0049	0.0014	6.51	0.41
	1520	15	20.94	0.08	0.62	0.03	0.79	0.05	0.67	0.02	0.46	0.01	0.0051	0.0012	6.42	0.26
	1540	15	21.01	0.07	0.62	0.02	0.79	0.03	0.67	0.01	0.46	0.01	0.0050	0.0006	6.43	0.12
	4010	15	20.96	0.10	0.60	0.02	0.79	0.02	0.67	0.03	0.47	0.01	0.0049	0.0012	6.49	0.28
	4020	15	20.98	0.10	0.61	0.01	0.79	0.02	0.67	0.02	0.47	0.01	0.0050	0.0007	6.44	0.17
	4040	15	20.98	0.10	0.61	0.01	0.79	0.02	0.67	0.01	0.47	0.01	0.0049	0.0005	6.45	0.09

AC: analytical condition (cf. Table A2); N: number of analyses; av and 1σ are average value and standard deviation, respectively (wt% for oxides; apfu for a_{Cr}; GPa for *P*)
* A few analyses of sample Nov-42 resulted in negative values of a_{Cr} and were therefore excluded for the calculation of the mean and standard deviation of a_{Cr} and *P*.

Table A4. Model relationships between analytical error (relative st. dev., *err*) and element concentration (*c*) calculated by fitting the results of the analytical test to a function of the type $err = a / \sqrt{c}$ (after Potts et al. 1983). Listed parameters are fitted *a* values for each oxide (wt%) or element (a.p.f.u.) relevant to single-clinopyroxene geobarometry and for each combination of analytical conditions (nA-peak s/bkg s).

	15-10/10	15-20/20	15-40/40	40-10/10	40-20/20	40-40/40
Al_2O_3	3.15	2.68	1.74	2.09	1.59	0.99
Al	0.64	0.54	0.35	0.42	0.32	0.20
Cr_2O_3	6.42	4.78	3.39	3.89	2.61	2.17
Cr	1.08	0.80	0.57	0.65	0.44	0.36
Na_2O	3.85	2.48	1.90	2.95	1.66	1.33
Na	1.02	0.65	0.50	0.77	0.43	0.35